

Sparse Tensor PCA via Tensor Decomposition for Unsupervised Feature Selection

Junjing Zheng, Xinyu Zhang, Weidong Jiang

Abstract—Recently, introducing Tensor Decomposition (TD) methods into unsupervised feature selection (UFS) has been a rising research point. A tensor structure is beneficial for mining the relations between different modes and helps relieve the computation burden. However, while existing methods exploit TD to minimize the reconstruction error of a data tensor, they don't fully utilize the interpretable and discriminative information in the factor matrices. Moreover, most methods require domain knowledge to perform feature selection. To solve the above problems, we develop two Sparse Tensor Principal Component Analysis (STPCA) models that utilize the projection directions in the factor matrices to perform UFS. The first model extends Tucker Decomposition to a multiview sparse regression form and is transformed into several alternatively solved convex subproblems. The second model formulates a sparse version of the family of Tensor Singular Value Decomposition (T-SVDs) and is transformed into individual convex subproblems. For both models, we prove the optimal solution of each subproblem falls onto the Hermitian Positive Semidefinite Cone (HPSD). Accordingly, we design two fast algorithms based on HPSD projection and prove their convergence. According to the experimental results on two original synthetic datasets (*Orbit* and *Array Signal*) and five real-world datasets, the two proposed methods are suitable for handling different data tensor scenarios and outperform the state-of-the-art UFS methods.

Index Terms—Tensor decomposition, Tensor PCA, Tucker decomposition, T-SVD, unsupervised feature selection.

I. INTRODUCTION

FEATURE Selection (FS) is a technique of selecting as few features (variables) as possible to meet the demands of a certain task [1], [2]. It is usually exploited as a pre-processing algorithm to relieve the computational burden and enhance interpretability by offering only the necessary features. According to the amount of supervised information during training, FS methods can be classified as supervised [3], semi-supervised [4], and unsupervised [5]. Among them, Unsupervised Feature Selection (UFS) is more challenging due to the unavailability of labels. To overcome the difficulty, most UFS methods apply learning methods including but not limited to principal component analysis (PCA [47]), spectral clustering, and graph-based learning. In this paper, we focus on PCA-based UFS methods.

In most UFS methods, data samples are vectorized, resulting in the *curse of dimensionality* [6] as well as data structure loss when dealing with *tensors*. As a natural extension of

Scenario	Visual	Example
Tube-wise		<ol style="list-style-type: none"> 1. snapshots of array signal [8], [10], [11]. 2. images and video [7], [12], [13].
Slice-wise		<ol style="list-style-type: none"> 1. time series with different channels [9], [14]–[16]. 2. multi-way tables in the area of psychometrics [17].

Fig. 1. Two scenarios for third-order data tensors. Assume each frontal slice is a sample. Different colors refer to different variables. This paper regards variables as features. UFS refers to unsupervised feature selection. Tube-wise scenario: elements within one fiber belong to one variable. Slice-wise scenario: elements within one horizontal slice belong to one variable.

matrix to store multi-way data samples, tensor is now a common processed object in various communities such as image processing [7], signal processing [8], and economical analysis [9]. A n^{th} -order tensor comprises n modes (also called ways), each containing several dimensions. The tensor structure contains rich information on the relations of modes and dimensions, which is beneficial for analyzing the features. To discuss these relations, the data organization should be first identified. This paper focuses on third-order tensors and summarizes two scenarios of data organization: tube-wise and slice-wise, as Fig. 1 shows. Different organizations lead to different interpretations of the relations.

To utilize the structure information, tensor-based UFS methods apply all kinds of Tensor Decomposition (TD) techniques [18]–[20]. Tensor decomposition aims to factorize a tensor into a product of several subtensors (or a sum of them), which has been considerably studied for decades since the famous Tucker decomposition [21] was proposed in 1964. As different definitions for tensor rank are established, various TD methods have been put forward, such as Higher-order Singular Value Decomposition (HOSVD) [12], CAN-DECOMP/PARAFAC decomposition (CPD) [22], [23], and Tensor Singular Value Decomposition (T-SVD) [24]. One purpose of TD is to mine the relations between modes and dimensions, which are naturally related to UFS. On the one hand, a TD method preserves the tensor structure for UFS. On the other hand, UFS helps to examine whether the relations learned by the TD method are accurate and interpretable. By minimizing the reconstruction error between a constructed tensor and its decomposition, tensor-based UFS methods successfully preserve the data structure information. However, most of these methods don't develop sparse TD and thus use the linear classifier matrix to perform UFS,

This work was supported by the National Science Foundation of China under Grants 61921001. The authors are with the College of Electronic Science and Technology, National University of Defense Technology, Changsha 410073, China. (Corresponding author: Xinyu Zhang, Jiang Weidong) Emails: {zjj20212035@163.com; zhangxinyu90111@163.com; jwd2232@vip.163.com.

making it difficult to fully utilize the learned element relations in the factor matrices. To address this problem, we start by finding the compact representations of the factor matrices. As is all known, TD methods are also viewed as ways to achieve Tensor Principal Component Analysis (TPCA) [12], [25]. The principal components have the greatest variance among data samples on a global manifold. Their directions describe the feature necessity during the projection onto the manifold. Therefore, the key to finding the interpretable and discriminative features could be hidden in TPCA.

In terms of performing linear projection, the current TPCA methods can be roughly divided into two types: 1) Tuckers-based TPCA [12], [26], [27]: TPCA based on the *direction-unfolding products* defined by Tucker decomposition and its variation, and 2) T-SVDs-based TPCA [28]–[30]: TPCA based on the \star_M *product* defined by T-SVD and its generalization T-SVDM [31]. These two types of TPCA methods perform truncated SVD on different levels of a tensor to obtain factor matrices. Most Tuckers-based TPCA methods unfold a tensor into a matrix along one mode and perform direction-unfolding products (An important exception will be mentioned in Section II-C). They regard the elements in the same dimension as a whole during projection. T-SVDs-based TPCA methods conduct truncated SVD slice-by-slice based on \star_M product. They assign each element a weight and have a more delicate description of the element relations. Due to the difference in products, the two types of TPCA are suitable for handling different scenarios of data organization in UFS. Before these TPCA methods are applied to UFS, they need the guidance of sparsity constraints to ensure the preservation of only the necessary relations. In addition, the subproblems in the TPCA models are non-convex. Therefore, this paper develops a sparse version for each type of TPCA method and transforms the model into convex optimization subproblems. The proposed methods directly utilize the learned relations to perform UFS.

Based on the above introduction, we summarize our work as follows:

- We deduce a sparse version of Tuckers-based TPCA called *Sparse Tensor PCA based on Direction-unfolding Product (STPCA-DP)*. We transform the model into several alternatively solved convex subproblems and prove the optimal solution falls onto the Hermitian Positive Semidefinite (HPSD) Cone. We design a fast algorithm to solve this model and prove its convergence.
- We deduce a sparse version of T-SVDs-based TPCA called *Sparse Tensor PCA based on \star_M Product (STPCA-MP)*. We transform the model into several individual convex subproblems and prove the optimal solution falls onto the HPSD Cone. Also, We design a fast algorithm to solve the model and prove its convergence.
- In the background of unsupervised feature selection, we design two synthetic datasets: Orbit and Array Signal, corresponding to slice-wise and tube-wise tensors, respectively. We perform experiments on these two synthetic datasets and the other five real-world datasets to explore the relations between data organization and the proposed methods. The experimental results show that the proposed two methods outperform other comparative methods in

different scenarios respectively.

II. RELATED WORK

In this section, we introduce notations used throughout the paper, and research revolving around tensor decomposition, tensor PCA, and UFS.

A. Notations

1) *Basic Symbols*: In most cases, We use capital letters (e.g. A) to denote sets, except the common ones like integer set \mathbb{Z} , the real numbers set \mathbb{R} and the complex numbers set \mathbb{C} . Especially, H_+^d stands for Hermitian Positive Semidefinite Cone for $d \times d$ matrices, and Φ is the empty set. For an integer n , $[n]$ represents the set $[1, 2, 3, \dots, n]$. $\#(A)$ stands for the number of elements in the set A . A set with the superscript "o" has ordered elements, which means $A^o = \{1, 2, 3\} \neq B^o = \{1, 3, 2\}$.

We use lowercase letters (e.g. a) to denote scalars, boldface lowercase letters (e.g. \mathbf{a}) to denote vectors, boldface capital letters (e.g. \mathbf{A}) and Euler script letters (e.g. \mathcal{A}) to denote tensors. For a n^{th} -order tensor $\mathcal{A} \in \mathbb{C}^{d_1 \times d_2 \times \dots \times d_n}$, its (i_1, i_2, \dots, i_n) -th element is denoted by $\mathcal{A}_{i_1 i_2 \dots i_n}$ (For a matrix, the counterpart will be $\mathbf{A}_{i_1 i_2}$). For a matrix \mathbf{A} , its row vectors are denoted by $\mathbf{A}_{j,:}$ or boldface lowercase letters \mathbf{a}^j . The column vectors are denoted by $\mathbf{A}_{:,j}$ or boldface lowercase letters \mathbf{a}_j .

We denote the transpose, the conjugation, and the conjugate transpose of a matrix as \mathbf{A}^T , \mathbf{A}^* and \mathbf{A}^H , respectively. We denote the trace of a square matrix by $Tr(\mathbf{A})$. The rank of a matrix is denoted by $rank(\mathbf{A})$. A vector that contains the diagonal elements of \mathbf{A} is denoted by $diag(\mathbf{A})$. We denote Frobenious norm, nuclear norm and $\ell_{2,1}$ norm by $\|\mathbf{A}\|_F$, $\|\mathbf{A}\|_*$, and $\|\mathbf{A}\|_{2,1}$ respectively. The nuclear norm is defined as the sum of singular values. We calculate ℓ_2 -norm of the column vectors in a matrix, then sum them to obtain its $\ell_{2,1}$ -norm. We denote the Kronecker product by \otimes .

2) *Tensor Operations*: Now we introduce some tensor operations.

a) Tensor Structure

There are two kinds of common subtensor structures for third-order tensors: *fibers* and *slices*. A fiber is obtained by fixing every index but one in a tensor. For a tensor $\mathcal{A} \in \mathbb{C}^{d_1 \times d_2 \times d_3}$, fibers can be classified into column (mode-1) fibers $\mathcal{A}_{:,i_2 i_3}$, row (mode-2) fibers $\mathcal{A}_{i_1, : i_3}$, and tube (mode-3) fibers $\mathcal{A}_{i_1 i_2, :}$, as shown in Fig. 2 (a)(b)(c). A slice is a two-dimensional section obtained by fixing every index but two in a tensor. According to orientation, slices can be divided into frontal slices $\mathcal{A}_{:,:,i_3}$, lateral slices $\mathcal{A}_{:,i_2,:}$ and horizontal slices $\mathcal{A}_{i_1, :, :}$, as shown in Fig. 2 (d)(e)(f). The transpose of a third-order tensor is denoted by \mathcal{A}^T , which is defined as $(\mathcal{A}^T)_{:, :, i_3} = (\mathcal{A}_{:, :, i_3})^T$. \mathcal{A}^H is similarly defined.

b) Tensor unfolding

For tensor unfolding, we apply the methodology in [27], which is called *direction unfolding* in this paper.

Given a n^{th} -order tensor $\mathcal{A} \in \mathbb{C}^{d_1 \times d_2 \times \dots \times d_n}$, two sets $L = \{l_1, l_2, \dots, l_q\}$ ($l_1 < l_2 < \dots < l_q, q \in \mathbb{Z}$) and $R =$

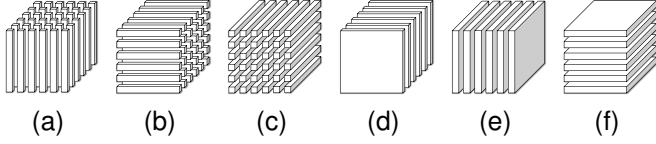


Fig. 2. Fibers and slices of a third-order tensor. (a) column fibers. (b) row fibers. (c) tube fibers. (d) frontal slices. (e) lateral slices. (f) horizontal slices.

$\{r_1, r_2, \dots, r_{n-q}\}$ ($r_1 < r_2 < \dots < r_q$) that satisfy $L \cup R = [n]$ and $L \cap R = \Phi$, then we can unfold \mathcal{A} into a matrix $\mathbf{A}_{(L \times R)} \in \mathbb{C}^{m_1 \times m_2}$ ($m_1 = \prod_{k \in L} d_k, m_2 = \prod_{k \in R} d_k$), where

$$\begin{aligned} (\mathbf{A}_{(L \times R)})_{jk} &= \mathcal{A}_{i_1 \dots i_n}, \\ j &= 1 + \sum_{c=1}^{n-q} \left[(i_{l_c} - 1) \prod_{c'=1}^{c-1} I_{l_{c'}} \right], \\ k &= 1 + \sum_{p=1}^q \left[(i_{r_p} - 1) \prod_{p'=1}^{p-1} I_{r_{p'}} \right]. \end{aligned} \quad (1)$$

Since R is accordingly determined given L , we can simplify $\mathbf{A}_{(L \times R)}$ with \mathbf{A}_L . When $L = \{k\}$ ($k \in [n]$) (e.g. $\mathbf{A}_{(1)}$), the unfolding progress is known as the famous k -mode unfolding, which we call **single-direction unfolding** in this paper. When L contains more than one element, we call the corresponding operation: **multiple-direction unfolding**. For an unfolded tensor $\mathbf{A}_{(L)}$, we use $fold(\mathbf{A}_{(L)})$ to fold it back to the original tensor.

c) Higher-order linear algebra framework of Tuckers

Based on direction unfolding, Tuckers' higher-order linear algebra framework can be defined with the following two types of direction-unfolding products.

- **Direction-unfolding inner product:** Given a direction set $L = \{l_1, l_2, \dots, l_q\}$, the direction-unfolding inner product between two tensors $\mathcal{A} \in \mathbb{C}^{d_1 \times \dots \times d_{l_1} \times \dots \times d_{l_q} \times \dots \times d_n}$ and $\mathcal{U} \in \mathbb{C}^{m \times d_{l_1} \times \dots \times d_{l_q}}$ is defined as

$$\begin{aligned} \mathcal{V} &= \mathcal{A} \times_L \mathcal{U} \\ &= fold(\mathbf{U}_{(1)} \times \mathbf{A}_L) \in \mathbb{C}^{d'_1 \times \dots \times d'_n}, \\ \mathcal{V}_{i_1 \dots j_1 \dots 1 \dots 1 \dots i_n} &= \sum_{k=1}^q \sum_{i_k=1}^{d_k} \mathcal{A}_{i_1 \dots i_{l_1} \dots i_{l_q} \dots i_n} \mathcal{U}_{j i_{l_1} i_{l_2} \dots i_{l_q}}, \\ d'_k &= \begin{cases} d_k, & \text{if } k \notin L, \\ m, & \text{if } k = l_1, \\ 1, & \text{if } k \in L \setminus \{l_1\}. \end{cases} \end{aligned} \quad (2)$$

A series of sequential non-overlapping direction-unfolding inner products are denoted by $\mathcal{L}_{\{\mathcal{U}^{(k)}, L_k\}}^\times(\cdot)$, where $L_i \cap L_j = \Phi$ ($i \neq j$). When L contains only one direction (or multiple directions), we call the corresponding product **single-direction product** (or **multiple-direction product**).

- **Direction-unfolding outer product:** Oppositely, we can define the direction-unfolding outer product given the

above \mathcal{U} and \mathcal{V} :

$$\tilde{\mathcal{A}} = \mathcal{V} \circ_L \mathcal{U} = fold(\mathbf{U}_{(1)}^H \times \mathbf{V}_L). \quad (3)$$

$\tilde{\mathcal{A}}$ can be viewed as a reconstruction of \mathcal{A} and is therefore usually not equal to \mathcal{A} . We denote a series of direction outer products by $\mathcal{L}_{\{\mathcal{U}^{(k)}, L_k\}}^\circ(\cdot)$.

d) Higher-order linear algebra framework of T-SVDs

In the framework of T-SVDs, the tensor-tensor product between third-order tensors is achieved by \star_M product. Given a third-order tensor $\mathcal{A} \in \mathbb{C}^{d \times m \times n}$, we first denote a tensor in the transform domain specified by an invertible matrix $\mathbf{M} \in \mathbb{C}^{n \times n}$:

$$\hat{\mathcal{A}} := \mathcal{A} \times_3 \mathbf{M}. \quad (4)$$

Then, given another tensor $\mathcal{B} \in \mathbb{C}^{m \times l \times n}$, $\mathcal{A} \star_M \mathcal{B} = \mathcal{C}$ is defined as

$$\begin{aligned} \hat{\mathcal{C}}_{:::,i} &= \hat{\mathcal{A}}_{:::,i} \hat{\mathcal{B}}_{:::,i}, \quad i = 1, 2, \dots, n, \\ \mathcal{C} &= \hat{\mathcal{C}} \times_3 \mathbf{M}^{-1} \in \mathbb{C}^{d \times l \times n}. \end{aligned} \quad (5)$$

From now on, we use $\hat{\mathcal{A}}$ to denote the result of $\mathcal{A} \times_3 \mathbf{M}$. The \star_M product is a slice-by-slice operation and is thus orientation-dependent. Different orientations of the tensor will lead to different results.

The identity tensor \mathcal{I} under \star_M satisfies

$$\mathcal{A} \star_M \mathcal{I} = \mathcal{I} \star_M \mathcal{A}^H = \mathcal{A}. \quad (6)$$

Each frontal slice of $\hat{\mathcal{I}}$ is an identity matrix \mathbf{I} .

The conjugate transpose of $\mathcal{A} \in \mathbb{C}^{d \times m \times n}$ under \star_M is defined as:

$$\left(\hat{\mathcal{A}}^H \right)_{:::,i} = \left(\hat{\mathcal{A}}_{:::,i} \right)^H, \quad i = 1, \dots, n, \quad (7)$$

which makes sure that $\mathcal{A}^H \star_M \mathcal{B}^H = (\mathcal{B} \star_M \mathcal{A})^H$. We can further define a \star_M -orthogonal tensor $\mathcal{A} \in \mathbb{C}^{m \times m \times n}$ if

$$\mathcal{A}^H \star_M \mathcal{A} = \mathcal{A} \star_M \mathcal{A}^H = \mathcal{I}. \quad (8)$$

B. Sparse PCA (SPCA)

To obtain sparse weights and achieve better interpretability, Sparse PCA (SPCA) [32] was proposed by adding ridge and lasso constraints to a self-contained regression form of PCA:

$$\begin{aligned} \min_{\mathbf{U}, \mathbf{Q}} \quad & \|\mathbf{X} - \mathbf{U}\mathbf{Q}^T \mathbf{X}\|_F^2 + \alpha \sum_{j=1}^k \|\mathbf{q}_j\|_2^2 + \beta \sum_{j=1}^k \|\mathbf{q}_j\|_1 \\ \text{s.t.} \quad & \mathbf{U}^T \mathbf{U} = \mathbf{I}_k, \end{aligned} \quad (9)$$

where \mathbf{Q} is a relaxed transform matrix. PCA can be seen as a special case of SPCA where $\mathbf{Q} = \mathbf{U}$.

SPCA makes it possible to exploit principal components to distinguish the necessary features. Our proposed methods are rooted in SPCA's deduction.

C. Tuckers and tensor PCA

Tucker decomposition was initially proposed to mine the mode relations in third-order tensors [21]. Later, [12] extends Tucker's linear algebra framework to higher-order tensors and proposes HOSVD. Recently, [27] introduces multiple-direction unfolding and proposes to decompose a n^{th} -order tensor $\mathcal{A} \in \mathbb{R}^{d_1 \times \dots \times d_n}$ as :

$$\mathcal{A} \approx \mathcal{L}_{\{U^k, L_k\}}^{\circ}(\mathcal{C})(k \in [s], s \leq n), \quad (10)$$

where $\mathcal{C} \in \mathbb{R}^{m_1 \times m_2 \times \dots \times m_n}$ is a low-dimensional tensor known as *core tensor*, L_k are several non-overlapping direction sets, and U^k are tensors whose 1-mode unfolding matrix is row-orthogonal. Another example of putting constraints on Tucker decomposition is CP decomposition (CPD) [22], [23] whose core tensor is supersymmetric with superdiagonal elements being 1. All of these TD methods are part of the family of Tuckers.

There have been two major advances in Tuckers-based TPCA: Multilinear PCA (MPCA) [26] and Multiview-PCA [27]. MPCA proposes to iteratively update the factor matrices obtained from the single-direction unfolding of the tensor while maximizing the total tensor scatter. Multiview-PCA [27] extends this principle to the one based on multiple-direction unfolding and successfully captures the large variance along the 3-mode in tube-wise tensors. Although a sparse version of MPCA has been put forward in [33] and achieves good performance, the counterpart of Multiview-PCA, which has the potential to deal with slice-wise and tube-wise data for UFS, remains absent. Therefore, this paper establishes a sparse model with the basis of Multiview-PCA.

D. T-SVDs and tensor PCA

By exploiting $\star_{\mathbf{M}}$ product, T-SVDs decompose a third-order tensor $\mathcal{A} \in \mathbb{C}^{d_1 \times d_2 \times d_3}$ into:

$$\mathcal{A} = \mathcal{U} \star_{\mathbf{M}} \mathcal{S} \star_{\mathbf{M}} \mathcal{V}^H, \quad (11)$$

where $\mathcal{U} \in \mathbb{C}^{d_1 \times d_1 \times d_3}$, $\mathcal{V} \in \mathbb{C}^{d_2 \times d_2 \times d_3}$ are $\star_{\mathbf{M}}$ -unitary, and $\mathcal{S} \in \mathbb{C}^{d_1 \times d_2 \times d_3}$ is a *f-diagonal* tensor whose frontal slices are diagonal. The decomposition is called T-SVD [24] when \mathbf{M} is the DFT matrix and T-SVDM [31] in a usual case.

[28] is the first study to point out the relation between T-SVD and tensor PCA. It applies T-SVD to compress the human-face images with a pre-rotation of the data tensor. [31] further extends this idea to T-SVDM. [29] points out the importance of utilizing the orientation-dependence of T-SVDs to obtain information from different directions. Inspired by them, we derive a sparse model for T-SVDM and utilize the orient-dependence property in UFS.

E. Tensor-based unsupervised feature selection

Tensor-based unsupervised feature selection is still a developing research point. Most of the existing methods require domain knowledge. For example, [20] proposes an image-transformation-based feature selection method, aiming at vehicle detection. [34] constructs a multi-omics data tensor and exploits feature selection criterion designed using the

knowledge in bioinformatics. There are, though, some methods designed for general cases. GRLTR [35] combines graph regularization and tensor tubal rank constraint to simultaneously preserve global and local information. However, it still requires vectorization. CPUFS [18] derives a model based on CPD and effectively preserves the tensor structure by minimizing the reconstruction error. It is a successful exploration of tensor-based UFS. However, CPUFS applies spectral clustering and utilizes the linear classifier matrix to perform UFS, leading to insufficient utilization of the information in factor matrices. Besides, the constructed graph in CPUFS needs the number of classes as prior knowledge and can be unreliable due to noise features.

Recently, developing sparse PCA (SPCA) models for UFS appears to be a new trend [36]–[39]. PCA-like methods don't rely on the construction of graphs and any label information. By global manifold learning, they can preserve the data structure. More importantly, they use the sparse factor matrix to perform UFS and achieve better average performance. Since they maximize the variance of data samples in the projected space, the weights in the factor matrix will have more interpretability and contain discriminative information. Unfortunately, these methods are non-tensor-based. Therefore, this paper explores suitable ways of developing effective TPCA methods for UFS.

III. METHODOLOGY

In this section, we derive two sparse tensor PCA models based on Tuckers' and T-SVDs' frameworks.

A. Sparse Tensor PCA based on Direction Unfolding: STPCA-DP

By exploiting the Tuckers' framework, we derive a model called *Sparse Tensor PCA based on Direction-unfolding Product (STPCA-DP)*.

1) *Model*: Suppose we have t centralized tensor samples $\{\mathcal{X}^1, \mathcal{X}^2, \dots, \mathcal{X}^t\}$ where $\mathcal{X}^i \in \mathbb{C}^{d_1 \times \dots \times d_n}$. Given several direction sets $\{L_k, k \in K, \#(K) = s \leq n\}$ ($L_i \cap L_j = \Phi(i \neq j)$), where each direction set $L_k = \{l_{1k}^k, l_{2k}^k, \dots, l_{q_k}^k\} \subseteq [n]$, a multiview sparse regression form of TPCA based on direction-unfolding product can be formulated as follows:

$$\begin{aligned} \min_{\mathcal{U}^k, \mathcal{Q}^k} \quad & \sum_{i=1}^t \|\mathcal{X}^i - \mathcal{X}^i \times_{L_1} \mathcal{Q}^1 \circ_{L_1} \mathcal{U}^1 \dots \times_{L_s} \mathcal{Q}^s \circ_{L_s} \mathcal{U}^s\|_F^2 \\ & + \alpha \sum_{k=1}^s \sum_{j=1}^m \left\| \left(\mathbf{Q}_{(1)}^k \right)_{j,:} \right\|_2^2 + \beta \sum_{k=1}^s \sum_{j=1}^m \left\| \left(\mathbf{Q}_{(1)}^k \right)_{j,:} \right\|_1, \\ \text{s.t.} \quad & \left\{ \left(\mathbf{U}_{(1)}^k \right)_{j,:}, j \in [m] \right\} \text{ are orthonormal,} \end{aligned} \quad (12)$$

where $\mathcal{Q}^k \in \mathbb{C}^{m \times d_{l_1^k} \times \dots \times d_{l_{q_k}^k}}$ and $\mathcal{U}^k \in \mathbb{C}^{m \times d_{l_1^k} \times \dots \times d_{l_{q_k}^k}}$ ($m \leq \prod_{j \in [q]} d_{l_j^k}$). $\alpha > 0$ and $\beta > 0$ are regularization parameters.

The operation $\mathcal{X}^i \times_{L_k} \mathcal{Q}^k \circ_{L_k} \mathcal{U}^k$ is equivalent to $\mathcal{X}^i \times_{L_k} \mathbf{A}^k$, where $\mathbf{A}_{L_k}^k = \left(\mathbf{U}_{(1)}^k \right)^H \mathbf{Q}_{(1)}^k$. We call \mathbf{A}^k **reconstruction tensor**. It is proven in [27] that \times_{L_k} has permutation invariance. Therefore, we can first fix $\{\mathcal{U}^k, \mathcal{Q}^k, k \neq e\}$

and discuss the optimization of $\{\mathcal{U}^e, \mathcal{Q}^e\}$. Denote $\mathcal{Y}^i = \mathcal{L}_{\{\mathcal{A}^k, L_k, k \neq e\}}^\times(\mathcal{X}^i)$, we obtain

$$\begin{aligned} \min_{\mathcal{U}^e, \mathcal{Q}^e} & \sum_{i=1}^t \|\mathcal{X}^i - \mathcal{Y}^i \times_{L_e} \mathcal{Q}^e \circ_{L_e} \mathcal{U}^e\|_F^2 \\ & + \alpha \sum_{j=1}^m \left\| \left(\mathbf{Q}_{(1)}^e \right)_{j,:} \right\|_2^2 + \beta \sum_{j=1}^m \left\| \left(\mathbf{Q}_{(1)}^e \right)_{j,:} \right\|_1, \quad (13) \\ \text{s.t.} & \left\{ \left(\mathbf{U}_{(1)}^e \right)_{j,:}, j \in [m] \right\} \text{ are orthonormal,} \end{aligned}$$

Further, (13) can be reformulated in a matrix form as follows:

$$\begin{aligned} \min_{\mathbf{U}_{(1)}^e, \mathbf{Q}_{(1)}^e} & \sum_{i=1}^t \left\| \mathbf{X}_{L_e}^i - \left(\mathbf{U}_{(1)}^e \right)^H \mathbf{Q}_{(1)}^e \mathbf{Y}_{L_e}^i \right\|_F^2 \\ & + \lambda \left\| \left(\mathbf{Q}_{(1)}^e \right)^H \right\|_{2,1}, \quad (14) \\ \text{s.t.} & \mathbf{U}_{(1)}^e \left(\mathbf{U}_{(1)}^e \right)^H = \mathbf{I}, \end{aligned}$$

where $\lambda > 0$ is the regularization parameter, and $\ell_{2,1}$ -norm is utilized to achieve both the goals of ℓ_1 -norm and ℓ_2 -norm [39]. For (14), we have the following theorem:

Theorem 1. *Let \mathbf{U}_{opt} and \mathbf{Q}_{opt} be the optimal solution to problem (14), Then $(\mathbf{U}_{opt})^H \mathbf{Q}_{opt} \in H_+^{\prod_{j=1}^{q_e} d_{l_j^e}}$.*

Proof. To simplify the deduction, we first rewrite the problem with compact symbols:

$$\begin{aligned} \min_{\mathbf{U}, \mathbf{Q}} & \sum_{i=1}^t \|\mathbf{X}^i - \mathbf{U}^H \mathbf{Q} \mathbf{Y}^i\|_F^2 + \lambda \|\mathbf{Q}^H\|_{2,1}, \quad (15) \\ \text{s.t.} & \mathbf{U} \mathbf{U}^H = \mathbf{I}_k. \end{aligned}$$

Since \mathbf{X}^i is the unfolding matrix of the i^{th} sample in \mathcal{X} , $\sum_{i=1}^t \mathbf{X}^i (\mathbf{X}^i)^H = \mathbf{X}_{L_e} \mathbf{X}_{L_e}^H$. Similarly, $\sum_{i=1}^t \mathbf{X}^i (\mathbf{Y}^i)^H = \mathbf{X}_{L_e} \mathbf{Y}_{L_e}^H$. Thus, we can rewrite the objection function as:

$$\begin{aligned} & Tr(\mathbf{X}_{L_e} \mathbf{X}_{L_e}^H) - \sum_{j=1}^k \left[Tr(\mathbf{u}^j \mathbf{X}_{L_e} \mathbf{Y}_{L_e}^H (\mathbf{q}^j)^H) - \frac{\lambda}{\|\mathbf{q}^j\|_2} \mathbf{q}^j (\mathbf{q}^j)^H \right. \\ & \left. + Tr(\mathbf{q}^j \mathbf{Y}_{L_e} \mathbf{X}_{L_e}^H (\mathbf{u}^j)^H) - Tr(\mathbf{q}^j \mathbf{Y}_{L_e} \mathbf{Y}_{L_e}^H (\mathbf{q}^j)^H) \right] \\ & = Tr(\mathbf{X}_{L_e} \mathbf{X}_{L_e}^H) - \sum_{j=1}^k \left(\mathbf{u}^j \mathbf{X}_{L_e} \mathbf{Y}_{L_e}^H (\mathbf{q}^j)^H - \frac{\lambda}{\|\mathbf{q}^j\|_2} \mathbf{q}^j (\mathbf{q}^j)^H \right. \\ & \left. + \mathbf{q}^j \mathbf{Y}_{L_e} \mathbf{X}_{L_e}^H (\mathbf{u}^j)^H - \mathbf{q}^j \mathbf{Y}_{L_e} \mathbf{Y}_{L_e}^H (\mathbf{q}^j)^H \right) \quad (16) \end{aligned}$$

if we view the above problem as a sum of k subproblems with respect to \mathbf{u}^j and \mathbf{q}^j . Then in each iteration, given a fixed \mathbf{u} (referring to \mathbf{u}_j), we can have each subproblem minimized at

$$\mathbf{q}_{opt}^* = \mathbf{u}^* \mathbf{X}_{L_e}^T \mathbf{Y}_{L_e}^* \left(\mathbf{Y}_{L_e}^* \mathbf{Y}_{L_e}^{*T} + \frac{\lambda}{\|\mathbf{q}\|_2} \mathbf{I}_d \right)^{-1}, \quad (17)$$

where $d = \prod_{j=1}^{q_e} d_{l_j^e}$. By substituting (17) back to (15) we can obtain

$$\begin{aligned} & \mathbf{u}_{opt} = \\ & \arg \min_{\mathbf{u} \mathbf{u}^H = \mathbf{I}} - \mathbf{u} \mathbf{X}_{L_e} \mathbf{Y}_{L_e}^H \left(\mathbf{Y}_{L_e} \mathbf{Y}_{L_e}^H + \frac{\lambda}{\|\mathbf{q}\|_2} \mathbf{I}_d \right)^{-1} \mathbf{Y}_{L_e} \mathbf{X}_{L_e}^H \mathbf{u}^H. \quad (18) \end{aligned}$$

Here, we assume that the reconstruction on \mathcal{X} doesn't change the directions of its principal components and only reassigns their weights, which means the singular vectors of \mathbf{Y}_{L_e} are equal to that of \mathbf{X}_{L_e} . Therefore, given the singular decomposition $\mathbf{X}_{L_e} = \mathbf{V} \mathbf{D} \mathbf{M}^H$ and $\mathbf{Y}_{L_e} = \mathbf{V} \mathbf{P} \mathbf{M}^H$, we have $\mathbf{u}_{opt}^j = s_j \mathbf{v}_j^H$ where $s_j = 1$ or -1 . Then, we obtain $(\mathbf{q}^j)_{opt} = s_j \frac{d_{jj} p_{jj}}{\|d_{jj}\|_2^2 + \lambda / \|\mathbf{q}^j\|_2} \mathbf{v}_j^H$.

Finally, we have

$$\mathbf{U}_{opt}^H \mathbf{Q}_{opt} = \sum_{j=1}^k (\mathbf{u}^j)^H \mathbf{q}^j = \mathbf{V} \Sigma \mathbf{V}^H \in H_+^{\prod_{j=1}^{q_e} d_{l_j^e}}, \quad (19)$$

where $\sigma = \frac{d_{jj} p_{jj}}{\|d_{jj}\|_2^2 + \lambda / \|\mathbf{q}^j\|_2} \geq 0$. In each iteration, $\mathbf{U}_{opt} \mathbf{Q}_{opt}^H$ satisfies (19). When Problem (15) is solved, (19) still holds. \square

Theorem 1 indicates that $\mathbf{A}_{L_e}^k \in H_+$ holds. Therefore, (14) can be transformed into

$$\begin{aligned} \min_{\mathbf{A}_{L_e}^e, \mathbf{Q}_{L_e}^e} & \sum_{i=1}^t \|\mathbf{X}_{L_e}^i - \mathbf{A}_{L_e}^e \mathbf{Y}_{L_e}^i\|_F^2 + \lambda \|\mathbf{Q}_{(1)}^e\|_{2,1}, \quad (20) \\ \text{s.t.} & \mathbf{A}_{L_e}^e \in S_+^b, \\ & \text{rank}(\mathbf{A}_{L_e}^e) < m, \end{aligned}$$

where $b = \prod_{j=1}^{q_e} d_{l_j^e}$ and $m < b$.

Because of the connection between $\mathbf{A}_{L_e}^e$ and $\mathbf{Q}_{(1)}^e$, $\|\mathbf{Q}_{(1)}^e\|_{2,1}$ is minimized as long as $\|\mathbf{A}_{L_e}^e\|_{2,1}$ is minimized. Therefore, we can utilize $\|\mathbf{A}_{L_e}^e\|_{2,1}$ instead for the convenience of optimization. Since the constraint of matrix rank is non-convex, we use the nuclear norm as its convex approximation and obtain:

$$\begin{aligned} \min_{\mathbf{A}_{L_e}^e} & \sum_{i=1}^t \|\mathbf{X}_{L_e}^i - \mathbf{A}_{L_e}^e \mathbf{Y}_{L_e}^i\|_F^2 + \lambda \|\mathbf{A}_{L_e}^e\|_{2,1} + \eta \|\mathbf{A}_{L_e}^e\|_*, \\ \text{s.t.} & \mathbf{A}_{L_e}^e \in H_+^b. \quad (21) \end{aligned}$$

Since $\mathbf{A}_{L_e}^e \in H_+^b$, $\|\mathbf{A}_{L_e}^e\|_* = Tr(\mathbf{A}_{L_e}^e)$ holds. Therefore, the model can be further written as:

$$\begin{aligned} \min_{\mathbf{A}_{L_e}^e} & \sum_{i=1}^t \|\mathbf{X}_{L_e}^i - \mathbf{A}_{L_e}^e \mathbf{Y}_{L_e}^i\|_F^2 + \lambda \|\mathbf{A}_{L_e}^e\|_{2,1} + \eta Tr(\mathbf{A}_{L_e}^e), \\ \text{s.t.} & \mathbf{A}_{L_e}^e \in H_+^b, \quad (22) \end{aligned}$$

which is a convex problem.

Eventually, considering all reconstruction tensors, we can write the model of STPCA-DP as follows:

$$\begin{aligned}
 \min_{\mathbf{A}_{L_k}^k} & \sum_{i=1}^t \|\mathcal{X}^i - \mathcal{L}_{\{\mathcal{A}^k, L_k\}}^{\times}(\mathcal{X}^i)\|_F^2 + \sum_{k=1}^s \lambda_k \|\mathbf{A}_{L_k}^k\|_{2,1} \\
 & + \sum_{k=1}^s \eta_k \text{Tr}(\mathbf{A}_{L_k}^k), \\
 \text{s.t. } & \mathbf{A}_{L_k}^k \in H_+^{\prod_{j=1}^{q_k} d_{L_j^k}}.
 \end{aligned} \quad (23)$$

2) *The application scope of STPCA-DP*: The application scope of STPCA-DP is determined by the direction sets. $\mathbf{A}_{L_k}^k$ reconstructs each dimension of the corresponding direction-unfolding matrix of the data tensor. The elements in $\mathbf{A}_{L_k}^k$ are weights that measure the importance of dimensions during reconstruction. Therefore, we can use these weights to score each dimension. Depending on the direction set L_k , the above dimensions can refer to dimensions (of a certain mode in the data tensor) or elements. Fig.3 gives a framework of how each version of STPCA-DP scores the features in a third-order data tensor. **Given 1 single-direction set $L = \{1\}$, we call it STPCA-DP-1SD.** **Given 2 single-direction sets $L_1 = \{1\}, L_2 = \{2\}$, we call it STPCA-DP-2SD.** **Given a multiple-direction set $L = \{1, 2\}$, we call it STPCA-DP-MD.**

For STPCA-DP-1SD, there is only one reconstruction tensor. It treats elements of the same dimension as a whole when it performs projection. In that way, STPCA-DP-1SD can learn the relations between each dimension of 1-mode and highly score the ones containing the largest amount of discriminative information. Naturally, STPCA-DP-1SD is suitable for slice-wise tensors where each dimension contains sample values of the same feature.

STPCA-DP-2SD integrates the information of the two modes by Kronecker product to score each element. The Kronecker product indicates that a selected feature needs to be highly scored in both modes, which is more likely in slice-wise tensors. Therefore, STPCA-DP-2SD is also suitable for slice-wise tensors. Additionally, STPCA-DP-2SD can also be applied to tube-wise tensors of special structures. We will discuss this further in the experiments.

STPCA-DP-MD applies multiple-direction unfolding to score each element. The corresponding product enables STPCA-DP-MD to utilize more weights to describe the feature relations in a tube-wise tensor at a price of higher computation complexity. Although STPCA-DP-MD can also be applied to a slice-wise tensor by summation, the obtained scores for each dimension of 1-mode are not correlated. Besides, unfolding multiple directions may lead to structure information loss.

3) *Algorithm*: Our idea to solve the above model is dividing (23) into s subproblems and solving them in each iteration. In each subproblem, We fix $\{\mathcal{A}_{L_k}, k \neq e\}$ and optimize \mathcal{A}_{L_e} until converge. To achieve this, We need to again rewrite (23) in terms of $\mathbf{A}_{L_e}^e$ with trace functions as:

$$\begin{aligned}
 \min_{\mathbf{A}_{L_e}^e} & \text{Tr}(\mathbf{A}_{L_e}^e \mathbf{S} (\mathbf{A}_{L_e}^e)^H) - 2\text{Tr}(\mathbf{S} \mathbf{A}_{L_e}^e) \\
 & + \lambda \text{Tr}(\mathbf{A}_{L_e}^e \mathbf{W}_e (\mathbf{A}_{L_e}^e)^H) + \eta \text{Tr}(\mathbf{A}_{L_e}^e), \\
 \text{s.t. } & \mathbf{A}_{L_e}^e \in H_+^b.
 \end{aligned} \quad (24)$$

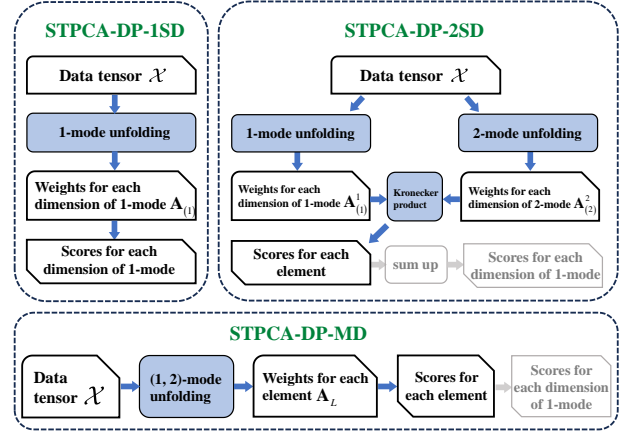


Fig. 3. A framework of how the STPCA-DPs score in the case of third-order tensor. The gray boxes stand for optional operations.

where $\mathbf{S} = \sum_{i=1}^t \mathbf{X}_{L_e}^i (\mathbf{Y}_{L_e}^i)^H$ and $\mathbf{W}_e \in \mathbb{R}^{b \times b}$ is a diagonal matrix whose j -th diagonal element is calculated by $(1 / (2\sqrt{\mathbf{a}_j^H \mathbf{a}_j + \epsilon_1}))$. Note that $\epsilon_1 > 0$ is a small positive number added to prevent $\sqrt{\mathbf{a}_j^H \mathbf{a}_j}$ from being zero.

With \mathbf{W}_e fixed, we take the derivative of the objective function and set its value equal to zero, then we can get

$$\mathbf{A}_{L_e}^e = \left(\mathbf{S} - \frac{\eta}{2} \mathbf{I}_b \right) (\mathbf{S} + \lambda \mathbf{W}_e + \epsilon_2 \mathbf{I}_b)^{-1}, \quad (25)$$

where ϵ_2 is also a small positive number used to prevent the possible irreversibility of $(\mathbf{S} + \lambda \mathbf{W}_e)$.

The next step is to project $\mathbf{A}_{L_e}^e$ onto the HPSD cone. We can achieve this by utilizing the HPSD projection operator $P_{H_+^b}(\mathbf{A})$ which, for an arbitrary square matrix $\mathbf{A} \in \mathbb{C}^{b \times b}$, is defined as:

$$\begin{aligned}
 P_{H_+^b}(\mathbf{A}) &= \Pi_{H_+^b}(\Pi_{H^b}(\mathbf{A})) \\
 &= \Pi_{H_+^b}\left(\frac{1}{2}(\mathbf{A} + \mathbf{A}^H)\right) \\
 &= \sum_{i=1}^b \max\{\sigma_i, 0\} (\mathbf{u}^i)^H \mathbf{u}^i,
 \end{aligned} \quad (26)$$

where $\sum_{i=1}^b \sigma_i \mathbf{u}_i^H \mathbf{u}_i$ is the eigenvalue decomposition of $\frac{1}{2}(\mathbf{A} + \mathbf{A}^H)$. Then $\mathbf{A}_{L_e}^e$ can be updated by

$$\mathbf{A}_{L_e}^e = P_{H_+^b}\left(\left(\mathbf{S} - \frac{\eta}{2} \mathbf{I}_b\right) (\mathbf{S} + \lambda \mathbf{W}_e + \epsilon_2 \mathbf{I}_b)^{-1}\right) \quad (27)$$

For the e -th subproblem, we iteratively update \mathbf{W}_e and $\mathbf{A}_{L_e}^e$ until converge. The algorithm stops when the objective function value of (23) reaches a stop criterion. We summarize the algorithm in Table 1.

B. Sparse Tensor PCA based on \star_M Product: STPCA-MP

By utilizing the linear algebra framework of T-SVDs, we derive another model called *Sparse Tensor PCA based on \star_M Product (STPCA-MP)*. Since T-SVDs are designed for third-order tensors, STPCA-MP is also restricted to third-order cases.

Algorithm 1 The optimization algorithm for STPCA-DP

Input: Centralized samples $\{\mathcal{X}^i \in \mathbb{C}^{d_1 \times \dots \times d_n}, i \in [t]\}$, multiple direction sets $\{L_k \subseteq [n], k \in K\}$, regularization parameters $\{\lambda_k, k \in K\}$ and $\{\eta_k, k \in K\}$.

Output: features corresponding to h indices of the modes determined by $\{L_k \subseteq [n], k \in K\}$.

- 1: Randomly initialize $\mathbf{A}_{L_k}^k \in H_+^d$ and calculate \mathbf{W}_k using the elements in $\mathbf{A}_{L_k}^k$.
- 2: **repeat**
- 3: **for** $e = 1, 2, \dots, \#(K)$ **do**
- 4: calculate $\mathbf{Y}_{L_e}^i = \mathcal{L}_{\{fold(\mathbf{A}_k), L_k, k \neq e\}}^\times(\mathcal{X}^i)$ and $\mathbf{S} = \sum_{i=1}^t \mathbf{X}_{L_e}^i (\mathbf{Y}_{L_e}^i)^H$.
- 5: Update $\mathbf{A}_{L_e}^e$ according to (27).
- 6: Update \mathbf{W}_e .
- 7: **end for**
- 8: **until** converge
- 9: initialize $\mathbf{P} = \mathbf{A}_{L_s}$
- 10: **for** $e = s - 1, s - 2, \dots, 2, 1$ **do**
- 11: $\mathbf{P} = \mathbf{P} \otimes \mathbf{A}_{L_e}^e$
- 12: **end for**
- 13: Sort $\|\mathbf{p}_j\|_2$ in descending order, then select features whose indices correspond to the h greatest $\|\mathbf{p}_j\|_2$. For slice-wise tensors, the scores will be obtained by first reshaping the vector containing $\|\mathbf{p}_j\|_2$ into a score map in the sample size and then summing up each row.

1) *Model:* Suppose a data tensor $\mathcal{X} \in \mathbb{C}^{d \times m \times n}$ containing n samples of size $d \times m$ is rotated given an order set D^o , so that the second mode is the dimension of samples. We denote the rotated data tensor by $\mathcal{X}_{D^o} \in \mathbb{C}^{q \times n \times p}$.

Based on (11), We can reduce the row dimensionality of each frontal slice in \mathcal{X}_{D^o} with $U^H \in \mathbb{C}^{k \times q \times p}$ consisting of truncated left singular matrices, and then reconstruct it by $\mathcal{U} \in \mathbb{C}^{d \times k \times p}$:

$$\begin{aligned} \mathcal{V} &= U^H \star_M \mathcal{X}_{D^o}, \\ \tilde{\mathcal{X}}_{D^o} &= \mathcal{U} \star_M \mathcal{V}, \end{aligned} \quad (28)$$

where $\mathcal{V} \in \mathbb{C}^{k \times n \times p}$, and $\tilde{\mathcal{X}}_{D^o} \in \mathbb{C}^{q \times n \times p}$. With the above observation, it is natural to come out with a sparse tensor PCA model based on T-SVDs:

$$\begin{aligned} \min_{\mathcal{U}, \mathcal{Q}} \quad & \|\mathcal{X}_{D^o} - \mathcal{U} \star_M \mathcal{Q}^H \star_M \mathcal{X}_{D^o}\|_F^2 + \alpha \sum_{j=1}^{pn} \left\| \left(\hat{\mathbf{Q}}_{(1)} \right)_{:,j} \right\|_2^2 \\ & + \beta \sum_{j=1}^{pn} \left\| \left(\hat{\mathbf{Q}}_{(1)} \right)_{:,j} \right\|_1, \\ \text{s.t.} \quad & \hat{U}_{:,i}^H \left(\hat{U}_{:,i} \right) = \mathbf{I}, i \in [p], \end{aligned} \quad (29)$$

where “ \star ” stands for the transform domain, e.g. $\hat{U} = U \times_3 M$. The same as STPCA-DP, we utilize $\ell_{2,1}$ -norm and rewrite the

problem in a matrix form:

$$\begin{aligned} \min_{\hat{\mathcal{A}}, \hat{\mathcal{Q}}} \quad & \sum_{i=1}^p \left\| \left(\hat{\mathcal{X}}_{D^o} \right)_{:,i} - \hat{U}_{:,i} \hat{\mathcal{Q}}_{:,i}^H \left(\hat{\mathcal{X}}_{D^o} \right)_{:,i} \right\|_F^2 \\ & + \lambda \sum_{j=1}^p \left\| \hat{\mathcal{Q}}_{:,i} \right\|_{2,1} \\ \text{s.t.} \quad & \hat{U}_{:,i}^H \left(\hat{U}_{:,i} \right) = \mathbf{I}, i \in [p], \end{aligned} \quad (30)$$

Similar to the deduction in STPCA-DP, it can be easily proven that $\hat{U}_{:,i} \hat{\mathcal{Q}}_{:,i}^H \in H_+^q$. Therefore, we make no further detailed description. **By defining $\mathcal{A} = \mathcal{U} \star_M \mathcal{Q}^H$, we end up with the model of STPCA-MP:**

$$\begin{aligned} \min_{\mathcal{A}} \quad & \|\mathcal{X}_{D^o} - \mathcal{A} \star_M \mathcal{X}_{D^o}\|_F^2 + \sum_{i=1}^p \lambda_i \|\hat{\mathcal{A}}_{:,i}\|_{2,1} \\ & + \sum_{i=1}^p \eta_i \text{Tr} \left(\hat{\mathcal{A}}_{:,i} \right), \\ \text{s.t.} \quad & \hat{\mathcal{A}}_{:,i} \in H_+^q, i \in [p]. \end{aligned} \quad (31)$$

In practice, the order set D^o can be either $\{1, 3, 2\}$ or $\{2, 3, 1\}$, each corresponding to the direction of 1-mode and 2-mode.

2) *The application scope of STPCA-MP:* When $M = \mathbf{I}$, STPCA-MP executes slice-by-slice operations on the rotated data tensor in the original domain. Specifying an order set, the i -th frontal slice of the rotated tensor contains the i -th vectors of a mode from all samples. Therefore, a set of score vectors can be obtained from \mathcal{A} . The concatenated score vectors form a map for each element. Fig. 4 gives a framework of how the STPCA-MPs score. **Given the order set $D^o = \{1, 3, 2\}$, we call the method STPCA-MP-Dir1** because it works along the dimensions of 1-mode. For a similar reason, **we call the method STPCA-MP-Dir2** given $D^o = \{2, 3, 1\}$.

Due to the separate operations on each slice, STPCA-MP can handle data tensors at a smaller computation cost compared to STPCA-DP-MD. The performance of STPCA-MP is determined by the information’s distribution direction, which will be discussed further in the experiments.

3) *Algorithm:* Rewrite Problem (31) with matrix multiplications as:

$$\begin{aligned} \min_{\hat{\mathcal{A}}} \quad & \sum_{i=1}^p \left\| \left(\hat{\mathcal{X}}_{D^o} \right)_{:,i} - \hat{\mathcal{A}}_{:,i} \left(\hat{\mathcal{X}}_{D^o} \right)_{:,i} \right\|_F^2 + \sum_{i=1}^p \lambda_i \|\hat{\mathcal{A}}_{:,i}\|_{2,1}, \\ & + \sum_{i=1}^p \eta_i \text{Tr} \left(\hat{\mathcal{A}}_{:,i} \right), \\ \text{s.t.} \quad & \hat{\mathcal{A}}_{:,i} \in H_+^q, i \in [p]. \end{aligned} \quad (32)$$

We can view Problem (32) as the summation of p subproblems, each of which can be separately solved. It can be observed that each subproblem is similar to that of STPCA-DP (Problem (22)). Therefore, we can update $\hat{\mathcal{A}}_{:,i}$ by the following expression:

$$\hat{\mathcal{A}}_{:,i} = P_{H_+^q} \left(\left(\mathbf{S} - \frac{\eta_i}{2} \mathbf{I}_q \right) \left(\mathbf{S} + \lambda_i \mathbf{W}_i + \epsilon_2 \mathbf{I}_q \right)^{-1} \right) \quad (33)$$

where $\mathbf{S} = \left(\hat{\mathcal{X}}_{D^o} \right)_{:,i} \left(\hat{\mathcal{X}}_{D^o} \right)_{:,i}^T$ and $\mathbf{W}_i \in \mathbb{R}^{q \times q}$ is a diagonal matrix whose j -th diagonal element is calculated

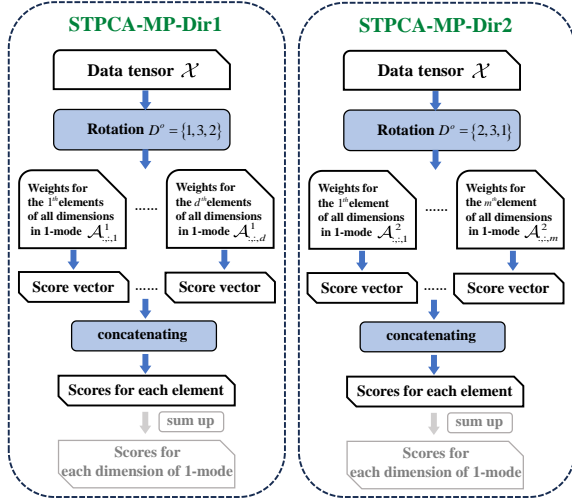


Fig. 4. A framework of how STPCA-MP scores in the case of third-order tensor. The gray boxes stand for optional operations.

Algorithm 2 The optimization algorithm for STPCA-MP

Input: A third-order centralized data tensor $\mathcal{X} \in \mathbb{C}^{d \times m \times n}$, the order sets D^o determining q , an invertible matrices $\mathbf{M} \in \mathbb{C}^{q \times q}$, regularization parameters $\{\lambda_i, \eta_i \mid i \in [q]\}$.

Output: h selected features.

- 1: Randomly initialize $(\tilde{\mathbf{A}})_{:,i} \in H_+^q$, transform \mathcal{X} into $\tilde{\mathcal{X}}$.
 - 2: **for** $i = 1, 2, \dots, q$ **do**
 - 3: revolve $\tilde{\mathcal{X}}$ with D^o and obtain $\tilde{\mathcal{X}}_{D^o}$.
 - 4: input $(\tilde{\mathcal{X}}_{D^o})_{:,i}$ and alternatively update $\hat{\mathbf{A}}_{:,i}$ and \mathbf{W}_i according to (33) until converge.
 - 5: Compute $\mathcal{A}_{:,i} = \hat{\mathbf{A}}_{:,i} \times_3 \mathbf{M}^{-1}$ and $\|\mathbf{a}_j\|_2 (j = 1, 2, \dots, q)$ as scores for each feature in the column fiber.
 - 6: **end for**
 - 7: Output a feature score map *Score*.
 - 8: Sort *Score* in descending order, and select features of the h greatest scores. For slice-wise tensor, the score for each dimension will be obtained by summation.
-

by $(1 / (2\sqrt{\hat{\mathbf{a}}_j^H \hat{\mathbf{a}}_j + \epsilon_1}))$. Each subproblem processes one column fiber of the rotated tensor. When a subproblem is solved, we can compute $\|\mathbf{a}_j\|_2 (j = 1, 2, \dots, q)$ as scores for each feature in that fiber. We summarized the algorithm in Algorithm 2.

IV. DISCUSSION

In this section, we analyze the proposed methods' convergence and computational complexity.

A. Convergence analysis

1) *Convergence analysis for STPCA-DP:* First, let us introduce a lemma [40]:

Lemma 1. For any nonzero vectors $\mathbf{a}, \mathbf{b} \in \mathbb{R}^{c \times 1}$, the following inequality holds:

$$\|\mathbf{a}\|_2 - \frac{\|\mathbf{a}\|_2^2}{2\|\mathbf{b}\|_2} \leq \|\mathbf{b}\|_2 - \frac{\|\mathbf{b}\|_2^2}{2\|\mathbf{b}\|_2}. \quad (34)$$

Based on **Lemma 1** and given $\{L_k, k \in K, \#(K) \leq n\}$ ($L_i \cap L_j = \Phi (i \neq j)$), we have the following theorem:

Theorem 2. the objective function value of Problem (23) is nonincreasing in each iteration of Algorithm 1 and can converge to a local minimum.

Proof. By fixing $\mathbf{A}_{L_k}^k (k \neq e)$, Problem (23) becomes convex for $\mathbf{A}_{L_e}^e$. For simplicity, we temporally use \mathbf{A} to replace $\mathbf{A}_{L_e}^e$. Denote the updated \mathbf{A} as $\tilde{\mathbf{A}}$ and fix \mathbf{W} . For problem (24), we have the following inequality

$$\begin{aligned} Tr(\tilde{\mathbf{A}}\mathbf{S}\tilde{\mathbf{A}}^H) - 2Tr(\mathbf{S}\tilde{\mathbf{A}}) + \lambda Tr(\tilde{\mathbf{A}}\mathbf{W}\tilde{\mathbf{A}}^H) + \eta Tr(\tilde{\mathbf{A}}) \\ \leq Tr(\mathbf{A}\mathbf{S}\mathbf{A}^H) - 2Tr(\mathbf{S}\mathbf{A}) + \lambda Tr(\mathbf{A}\mathbf{W}\mathbf{A}^H) \\ + \eta Tr(\mathbf{A}). \end{aligned} \quad (35)$$

Denote $J(\mathbf{A}) = Tr(\mathbf{A}\mathbf{S}\mathbf{A}^H) - 2Tr(\mathbf{S}\mathbf{A}) + \lambda Tr(\mathbf{A}\mathbf{W}\mathbf{A}^H) + \eta Tr(\mathbf{A})$ and $J(\tilde{\mathbf{A}})$ as the updated $J(\mathbf{A})$. Inequality (35) can be rewritten as

$$J(\tilde{\mathbf{A}}) + \lambda Tr(\tilde{\mathbf{A}}\mathbf{W}\tilde{\mathbf{A}}^H) \leq J(\mathbf{A}) + \lambda Tr(\mathbf{A}\mathbf{W}\mathbf{A}^H). \quad (36)$$

Adding the same item $\sum_{j=1}^d \lambda \epsilon / 2\sqrt{\mathbf{a}_j^H \mathbf{a}_j + \epsilon}$ to both sides of (36), we obtain

$$\begin{aligned} J(\tilde{\mathbf{A}}) + \lambda Tr(\tilde{\mathbf{A}}\mathbf{W}\tilde{\mathbf{A}}^H) + \sum_{j=1}^d \frac{\lambda \epsilon}{2\sqrt{\mathbf{a}_j^H \mathbf{a}_j + \epsilon}} \\ \leq J(\mathbf{A}) + \lambda Tr(\mathbf{A}\mathbf{W}\mathbf{A}^H) + \sum_{j=1}^d \frac{\lambda \epsilon}{2\sqrt{\mathbf{a}_j^H \mathbf{a}_j + \epsilon}}. \end{aligned} \quad (37)$$

At the meantime, we have

$$Tr(\mathbf{A}\mathbf{W}\mathbf{A}^H) = Tr(\mathbf{A}^H \mathbf{W} \mathbf{A}) = \sum_{j=1}^d \frac{\lambda \mathbf{a}_j^H \mathbf{a}_j}{2\sqrt{\mathbf{a}_j^H \mathbf{a}_j + \epsilon}}. \quad (38)$$

The same equality holds for $Tr(\tilde{\mathbf{A}}\mathbf{W}\tilde{\mathbf{A}}^H)$. We substituted (38) into (37) and get

$$J(\tilde{\mathbf{A}}) + \sum_{j=1}^d \frac{\lambda(\tilde{\mathbf{a}}_j^H \tilde{\mathbf{a}}_j + \epsilon)}{2\sqrt{\mathbf{a}_j^H \mathbf{a}_j + \epsilon}} \leq J(\mathbf{A}) + \sum_{j=1}^d \frac{\lambda(\mathbf{a}_j^H \mathbf{a}_j + \epsilon)}{2\sqrt{\mathbf{a}_j^H \mathbf{a}_j + \epsilon}}. \quad (39)$$

According to **Lemma 1**, we have

$$\sqrt{\tilde{\mathbf{a}}_j^H \tilde{\mathbf{a}}_j + \epsilon} - \frac{\tilde{\mathbf{a}}_j^H \tilde{\mathbf{a}}_j + \epsilon}{2\sqrt{\mathbf{a}_j^H \mathbf{a}_j + \epsilon}} \leq \sqrt{\mathbf{a}_j^H \mathbf{a}_j + \epsilon} - \frac{\mathbf{a}_j^H \mathbf{a}_j + \epsilon}{2\sqrt{\mathbf{a}_j^H \mathbf{a}_j + \epsilon}}. \quad (40)$$

Further, we can accumulate (39) from $j = 1$ to $j = d$. Considering $\lambda > 0$, we can get

$$\begin{aligned} \lambda \sum_{j=1}^d \sqrt{\tilde{\mathbf{a}}_j^H \tilde{\mathbf{a}}_j + \epsilon} - \lambda \sum_{j=1}^d \frac{\tilde{\mathbf{a}}_j^H \tilde{\mathbf{a}}_j + \epsilon}{2\sqrt{\mathbf{a}_j^H \mathbf{a}_j + \epsilon}} \\ \leq \lambda \sum_{j=1}^d \sqrt{\mathbf{a}_j^H \mathbf{a}_j + \epsilon} - \lambda \sum_{j=1}^d \frac{\mathbf{a}_j^H \mathbf{a}_j + \epsilon}{2\sqrt{\mathbf{a}_j^H \mathbf{a}_j + \epsilon}}. \end{aligned} \quad (41)$$

By summing (39) and (41), we have

$$J(\tilde{\mathbf{A}}) + \lambda \sum_{j=1}^d \sqrt{\tilde{\mathbf{a}}_j^H \tilde{\mathbf{a}}_j + \epsilon} \leq J(\mathbf{A}) + \lambda \sum_{j=1}^d \sqrt{\mathbf{a}_j^H \mathbf{a}_j + \epsilon}. \quad (42)$$

Finally, we can get the following inequality

$$J(\tilde{\mathbf{A}}) + \lambda \|\tilde{\mathbf{A}}\|_{2,1} \leq J(\mathbf{A}) + \lambda \|\mathbf{A}\|_{2,1}. \quad (43)$$

Since the objective function is bounded below by 0, the convergence of a single subproblem is guaranteed. This works for STPCA-DP-1SD and STPCA-DP-MD. For STPCA-DP-2SD, there remains the convergence of the whole optimization problem. Denote the objective function of the p^{th} iteration for $\mathbf{A}_{L_e}^e$ by $J_e \left((\mathbf{A}_{L_e}^e)_p \right)$, we have

$$J_e \left((\mathbf{A}_{L_e}^e)_{p+1} \right) \leq J_e \left((\mathbf{A}_{L_e}^e)_p \right). \quad (44)$$

When $\mathbf{A}_{L_e}^e$ is updated, we have

$$\begin{aligned} & \sum_{i=1}^t \left\| \mathbf{X}_{L_e}^i - (\mathbf{A}_{L_e}^e)_{p+1} \left(\mathcal{L}_{\{\mathcal{A}_{p+1}^e, L_k, k \neq e\}}^\times (\mathcal{X}^i) \right)_{L_e} \right\|_F^2 \\ &= \sum_{i=1}^t \left\| \mathbf{X}_{L_{e+1}}^i - (\mathbf{A}_{L_{e+1}}^{e+1})_p \left(\mathcal{L}_{\{\mathcal{A}_p^{e+1}, L_k, k \neq e+1\}}^\times (\mathcal{X}^i) \right)_{L_{e+1}} \right\|_F^2 \\ &\leq \sum_{i=1}^t \left\| \mathbf{X}_{L_e}^i - (\mathbf{A}_{L_e}^e)_p \left(\mathcal{L}_{\{\mathcal{A}_p^e, L_k, k \neq e\}}^\times (\mathcal{X}^i) \right)_{L_e} \right\|_F^2. \end{aligned} \quad (45)$$

Thus, when $\mathbf{A}_{L_e}^e$ is updated, we have:

$$J_{e+1} \left((\mathbf{A}_{L_{e+1}}^{e+1})_{p+1} \right) \leq J_e \left((\mathbf{A}_{L_e}^e)_{p+1} \right) \leq J_e \left((\mathbf{A}_{L_e}^e)_p \right), \quad (46)$$

which means the objective function value will be nonincreasing after $\mathbf{A}_{L_k}^k, k \in K$ are alternatively updated in each iteration. Since the objective function is bounded below by 0, it will eventually converge to a local minimum. \square

2) *Convergence analysis for STPCA-MP*: Given an order set, each subproblem of STPCA-MP has a similar form as STPCA-DP-MD. Therefore, the convergence of STPCA-MP is equivalent to that of STPCA-DP-MD, which is already guaranteed.

B. Computational complexity

In this section, we analyze the computational complexity of the proposed methods in the third-order tensor cases $\mathcal{X} \in \mathbb{C}^{d_1 \times d_2 \times n}$.

1) *Computational complexity of STPCA-DP*: For STPCA-DP, given the direction set $L = \{1\}$ (STPCA-DP-1SD), it requires $O(d_1^2 d_2 n)$ to compute the covariance matrix and $O(d_1^3)$ to update the reconstruction matrix (including computing the derivative and the HPSD projection). The computational complexity is $O(d_1^2 d_2 n + d_1^3 t)$. For STPCA-DP-2SD, the computational complexity is $O((d_1^2 d_2 n + d_1^3 t_1) + (d_2^2 d_1 n + d_2^3 t_2) t)$, where t_1 and t_2 are the number of iterations for solving subproblems, and t is the number of iterations for solving the whole problem. For STPCA-DP-MD, the computational complexity is $O((d_1 d_2)^2 n + (d_1 d_2)^3 t)$.

2) *Computational complexity of STPCA-MP*: For STPCA-MP, given the order set $D_{row}^o = \{1, 3, 2\}$, d_2 subproblems will be solved, each costing $O(d_1^2 n + d_1^3 t_i)$ ($i = 1, 2, \dots, d_2$). The total computational complexity is $O\left(\sum_{i=1}^{d_2} (d_1^2 n + d_1^3 t_i)\right)$. If the order set $D_{col}^o = \{2, 3, 1\}$, it takes $O\left(\sum_{i=1}^{d_1} (d_2^2 n + d_2^3 t_i)\right)$.

In conclusion, **the computational complexity of the proposed methods is linear to the number of samples**, which means the proposed methods will still be efficient when facing data tensors with numerous samples.

V. EXPERIMENT

In this section, we carry out experiments on synthetic data and real-world data to demonstrate the effectiveness and the application scope of our proposed methods. A comprehensive analysis is given in Section V-D, connecting all the experimental results and analyzing the application scope of the proposed methods. The codes related to our proposed methods and the experiments are given at <https://github.com/zjj20212035/STPCA.git>.

A. Experimental Settings

1) *Experimental environment*: All the experiments are conducted on a personal computer with a 2.20 GHz CPU and 64GB main memory under the environment of the Windows 11 operation system.

2) *Comparative methods*: We compare our proposed methods with some state-of-the-art tensor-based UFS methods as follows:

- **CPUFS** [18]: CPUFS is a tensor-based UFS method that combines CPD and spectral clustering to preserve the tensor structure as well as find a linear projection for classification.
- **CPUFSnn** [18]: CPUFSnn is a variation of CPUFS that considers the nonnegative constraints of the linear classifier and applies the projection gradient descent for optimization.
- **SOGFS** [40]: SOGFS is a non-tensor-based method that optimizes an adaptive graph to preserve the local geometrical structure of data.

We use *All Features* as a baseline method, which uses all features to perform clustering.

3) *Parameter settings*: For all methods, we tune the regularization parameters by a grid-search strategy. For graph-based methods, we set the number of k-nearest neighbors to 5. For CPUFS, the other parameters remain the default in the open code provided by CPUFS's authors. We set the maximal number of iterations of all methods to 200. For STPCA-MP, we set $\mathbf{M} = \mathbf{I}$.

4) *Evaluation methodology and metrics*: In part of the experiments, after a UFS method has finished selecting features, we evaluate its performance by first conducting K-means clustering and then mapping the obtained pseudo labels to the real labels by adopting the Kuhn-Munkres algorithm [41]. Due to the K-means' dependence on initialization, we repeat

the clustering 30 times. The clustering metrics we use are as follows:

- **ACC:** ACC is used to describe the accuracy of clustering, and is calculated according to (47) and (48), where n is the total number of samples, $map(i)$ denotes the clustering label of the i -th sample after mapping to the real label, and $label(i)$ represents the ground truth label. A larger ACC indicates better performance.

$$ACC = \frac{1}{n} \sum_{i=1}^n \delta(map(i), label(i)). \quad (47)$$

$$\delta(p, q) = \begin{cases} 1 & \text{if } p = q, \\ 0 & \text{otherwise.} \end{cases} \quad (48)$$

- **NMI [42]:** NMI is utilized to describe the mutual dependence between clustering results (after being mapped into the real labels) and ground truth labels. Given the clustering results \mathbf{m} and the ground truth labels \mathbf{l} (both include all samples), $I(\mathbf{m}, \mathbf{l})$ denotes the mutual information between \mathbf{m} and \mathbf{l} . $H(\mathbf{m})$ and $H(\mathbf{l})$ are the entropy of \mathbf{m} and \mathbf{l} respectively. The same as ACC, a larger NMI means better clustering performance.

$$NMI(\mathbf{m}, \mathbf{l}) = \frac{I(\mathbf{m}, \mathbf{l})}{\sqrt{H(\mathbf{m})H(\mathbf{l})}}. \quad (49)$$

In other experiments, to compare the stability of selecting discriminative features, we compute the following two metrics:

- **Proportion of correctly selected features (POC):** We define POC as the following ratio:

$$POC = \left(\sum_{i=1}^g c \right) / (h \times g), \quad (50)$$

where g is the number of regularization parameter combinations, $\sum_{i=1}^g c$ is the total number of correctly selected features, and h is the number of selected features at each execution. *POC reflects the stability of a UFS method in terms of selecting discriminative features.*

- **Proportion of the times of selecting all correct features (POTC):** We define POTC as the following ratio:

$$POTC = s/g, \quad (51)$$

where s is the times of selecting all correct features and g is the times of executions (also the number of regularization parameter combinations). *POTC reflects the accuracy of a UFS method in terms of selecting discriminative features.*

B. Datasets

1) *Two synthetic datasets:* We design two synthetic tensor datasets corresponding to slice-wise and tube-wise cases. **Due to the page limit, the detailed descriptions of these two datasets are given in the supplementary material.** The data are shared at <https://github.com/zjj20212035/STPCA.git>.

a) Orbit: **Orbit is an example of a slice-wise tensor.** We generate n -Dimensional hypersphere orbits with different radii

TABLE I
STATISTICS OF ORBIT DATASETS. EACH DATASET IS DESCRIBED BY A (#CHANNEL) × (LENGTH OF TIME SERIES) × (#SAMPLE) TENSOR. CLASSES ARE DIVIDED ACCORDING TO RADIUS.

Datasets	n	#Size	#Sample	#Class
3D Orbit	3	9×41	100	2
4D Orbit	4	12×41	100	2
5D Orbit	5	15×41	100	2

TABLE II
STATISTICS OF ARRAY SIGNAL DATASETS.

Case	#Size	#Sample	#Class	#(Units with errors)
1	10×10	800	4	0
2	10×10	800	2	4 or 5

measured in Euclidean distance. n channels in the data tensor are orbital-coordinate series, while others are Gaussian random sequences. Each channel is viewed as a feature. The statistics of the three datasets of Orbit are given in Table I.

b) Array Signal: **Array Signal is an example of a tube-wise tensor.** We design two cases: 1) Case 1: no measurement errors; 2) Case 2: random measurement errors on some units. For each case, we generate a series of snapshots of stationary targets with different directions of arrivals (DOAs) to form data tensors. Case 1 is a special case where each feature is correlated. We use it for clustering experiments where 4 DOAs are to be distinguished. For Case 2, we design four types of spatial distributions for the units with errors: random, horizontal, vertical, and rectangular. We compute POC and POTC in the experiments of Case 2 to see if the proposed methods can find out the units with errors. The statistics of the two cases are given in Table II.

2) *Real-world datasets:* We perform experiments on five real-world datasets: PIE [13], JAFFE [43], BreatMNIST [44], UCIHAR [45] and UCIDSA [46]. The statistical property is shown in Table III. PIE and JAFFE contain frontal facial images, labeled according to individuals and facial expressions respectively. BreastMNIST is a medical dataset of breast ultrasound images (We use the test set). We regard the above three data as tube-wise tensors. UCIHAR and UCIDSA are both human activity datasets sampled from different individuals. UCIDSA contains sensor signals and UCIHAR contains statistical features extracted from sensor signals. For UCIDSA, we use the first 25-second signals of the 9 sensors embedded on the torso while jumping and rowing and segment them into several samples. For UCIHAR, we use the test data related to sitting, standing, and laying. All data are normalized and bounded within $[-1, 1]$.

C. Synthetic experiment

1) *Experiment on Orbit dataset:* In this experiment, we conduct experiments on Orbit dataset. All regularization parameters go through a grid search in $\{10^{-4}, 10^{-3}, 10^{-2}, 10^{-1}, 1, 10^1, 10^2, 10^3, 10^4\}$. We select the top n features from the output for each parameter

TABLE III

STATISTICS OF DATASETS. 'h' STANDS FOR HEIGHT. 'w' STANDS FOR WIDTH. 's' STANDS FOR SENSOR. 't' STANDS FOR TIME. 'f' STANDS FOR FEATURE.

Type	Dataset	# Size	# Samples	# Classes
Tube-wise	PIE [13]	32×32 ($h \times w$)	1166	53
	JAFFE [43]	64×64 ($h \times w$)	213	7
	BreastMNIST [44]	28×28 ($h \times w$)	156	2
Slice-wise	UCIDSA [46]	9×125 ($s \times t$)	80	2
	UCIHAR [45]	561×9 ($f \times i$)	138	3

TABLE IV

RESULTS ON THREE ORBIT DATASETS.

Method	3D Orbits	4D Orbits	5D Orbits
CPUFS [18]	POC: 34.06%	POC: 35.70%	POC: 34.84%
	POTC: 2.19%	POTC: 0%	POTC: 0%
CPUFSnn [18]	POC: 36.90%	POC: 37.72%	POC: 35.50%
	POTC: 1.78%	POTC: 0.55%	POTC: 0%
STPCA-MP-Dir1	POC: 44.44%	POC: 38.89%	POC: 33.33%
	POTC: 44.44%	POTC: 33.33%	POTC: 33.33%
STPCA-MP-Dir2	POC: 50.62%	POC: 45.99%	POC: 35.31%
	POTC: 40.74%	POTC: 29.63%	POTC: 29.63%
STPCA-DP-1SD	POC: 100.00%	POC: 100.00%	POC: 100.00%
	POTC: 100.00%	POTC: 100.00%	POTC: 100.00%
STPCA-DP-2SD	POC: 79.01%	POC: 79.01%	POC: 79.01%
	POTC: 79.01%	POTC: 79.01%	POTC: 79.01%
STPCA-DP-MD	POC: 56.26%	POC: 41.98%	POC: 39.51%
	POTC: 39.51%	POTC: 39.51%	POTC: 39.51%

combination. The results are shown in Table IV. **The two STPCA-DP-SDs maintain stable discriminative-feature selection on all three Orbit datasets.** Generally, the proposed methods outperform CPUFS and CPUFSnn which can barely select all the correct features.

2) *Experiment on Array Signal dataset:* In this experiment, we conduct experiments for both cases in Array Signal dataset. CPUFS, CPUFSnn, and SOGFS are not included in this experiment because they are not designed to handle complex-number data. The regularization parameters go through a grid search in the range of $\{10^{-2}, 10^{-1}, 1, 10^1, 10^2\}$.

We randomly generate 50 data tensors for Case 1. For each tensor, we execute the algorithms and select the top-ranked 5 features (units) for clustering. Since k-means cannot directly cluster complex-number data, we use the amplitude and phase angle to represent each element instead. Table V shows the average ACC and NMI. **STPCA-DP-2SD and two STPCA-MPs have approximate clustering results, while STPCA-DP-MD performs relatively worse.**

We randomly generate 50 data tensors for each type of spatial distribution in Case 2. For each method, we conduct the algorithm, select the top-ranked 4 (or 5) features, and compute POC and POTC. The average POC and POTC are given in Table VI. **It can be seen that the performance of all methods is highly related to the spatial distributions of units with errors, which will be further discussed in Section V-D.**

3) *Clustering experiment on real-world data:* In this experiment, we perform clustering on four real-world datasets.

TABLE V

EXPERIMENTAL RESULTS FOR CASE 1 IN ARRAY SIGNAL DATASET (AVERAGE%±STD%).

Method	ACC(Average±std%)	NMI(Average±std%)
All Features	$41.58 \pm 2.74\%$	$26.65 \pm 3.75\%$
STPCA-DP-2SD	$51.23 \pm 2.44\%$	$46.48 \pm 2.05\%$
STPCA-DP-MD	$48.64 \pm 4.59\%$	$43.18 \pm 7.47\%$
STPCA-MP-Dir1	$52.37 \pm 1.84\%$	$47.31 \pm 2.18\%$
STPCA-MP-Dir2	$52.22 \pm 1.74\%$	$46.97 \pm 2.09\%$

The regularization parameters of all methods go through a grid search in $\{10^{-2}, 10^{-1}, 1, 10^1, 10^2\}$. We set the selected features to $\{50, 100, 150, 200, 250, 300\}$ on PIE [13], JAFFE [43], BreatMNIST [44], and UCIHAR [45]. The best results of all methods are given in Table VII. The detailed ACC and NMI curves are given in the supplementary material. **It can be seen that the proposed methods outperform other comparative methods in terms of average clustering performance.**

4) *POC and POTC on UCIDSA:* In this experiment, we compute POC and POTC on UCIDSA¹. The discriminative features correspond to the three peak points in the between-class variance (BCV) curve of UCIDSA. The experimental results are given in Table VII. **Among all methods, two STPCA-DPs have the most prominent performance.** Other proposed methods also outperform comparative methods because of the guidance of the discriminative information given by sparse factor matrices.

5) *Training time comparison:* In this experiment, we compare the training time of all comparative methods. The average training time and the computational complexity are given in Table VII. Among all methods, STPCA-MP has the least computation cost. **The training time of all proposed methods is insensitive to #(Sample).** When #(Feature) increases, tensor-based methods have a significant advantage over methods requiring data vectorization.

6) *Visualization:* In this experiment, we perform a visualization to compare the interpretability. The best results in terms of NMI on Array Signal, PIE, JAFFE, and BreastMNIST are visualized in Fig. 5. **Due to the direct utilization of sparse factor matrices, the features selected by the proposed methods are more interpretable than CPUFS.** On the human face data, STPCA-DP-MD and STPCA-MP select features that cover the regions of eyes, eyebrows, mouth, nose, and hair, etc.. On BreastMNIST, the features selected by the proposed methods tend to be grouped. On Array Signal, different choices of directions lead to the sensitivity of features with different spatial distributions, which will be further discussed in Section V-D.

7) *Convergence analysis:* In this experiment, we study the convergence of the proposed methods. Due to the page limit, we only show the converge curves of STPCA-DP-2SD and

¹Most comparative methods can select the three discriminative features on UCIDSA given certain regularization parameters and have no significant difference at clustering metrics. Therefore, we compute POC and POTC instead to better compare the performance.

TABLE VI
EXPERIMENTAL RESULTS FOR CASE 2 IN ARRAY SIGNAL DATASET (AVERAGE%±STD%).

Method	Random	Horizontal	Vertical	Rectangular
STPCA-DP-MD	POC: 78.05% ± 11.11% POTC: 64.72% ± 8.19%	POC: 74.54% ± 16.16% POTC: 72.40% ± 16.66%	POC: 72.61% ± 15.77% POTC: 71.76% ± 16.13%	POC: 69.36% ± 12.89% POTC: 68.56% ± 13.35%
STPCA-DP-2SD	POC: 27.62% ± 8.22% POTC: 0% ± 0%	POC: 26.90% ± 15.80% POTC: 6.80% ± 10.33%	POC: 29.14% ± 19.67% POTC: 5.92% ± 12.32%	POC: 38.76% ± 20.22% POTC: 36.00% ± 19.00%
STPCA-MP-Dir1	POC: 62.03% ± 12.78% POTC: 42.64% ± 12.33%	POC: 57.36% ± 19.72% POTC: 57.36% ± 19.72%	POC: 25.68% ± 19.74% POTC: 4.32% ± 11.16%	POC: 50.56% ± 22.50% POTC: 44.40% ± 25.29%
STPCA-MP-Dir2	POC: 61.54% ± 12.50% POTC: 43.04% ± 11.56%	POC: 26.83% ± 19.92% POTC: 3.20% ± 9.18%	POC: 57.60% ± 22.77% POTC: 57.60% ± 22.77%	POC: 50.56% ± 22.50% POTC: 44.40% ± 25.29%

TABLE VII
METRICS OF THE COMPARATIVE METHODS ON REAL-WORLD DATASETS. THE TRAINING TIME IS RECORDED IN SECONDS.

Method	PIE		JAFEE		BreastMNIST		UCIHAR		UCIDSA	
	ACC		ACC		ACC		ACC		POC	
All Feature	NMI	26.21	NMI	20.16	NMI	58.25	NMI	82.51	POTC	-
	TIME	-	TIME	-	TIME	-	TIME	-	TIME	-
SOGFS [40] $O(dn^2 + t(d^3t_1 + n^2m + ndm))$	ACC	28.22	ACC	24.88	ACC	61.45	ACC	81.38	POC	46.67
	NMI	53.01	NMI	10.01	NMI	4.55	NMI	76.95	POTC	20.00
	TIME	14.56	TIME	3273.74	TIME	28.50	TIME	3826.59	TIME	10.30
CPUFS [18] $O(d_1nc^2 + d_2nc^2 + d_1d_2nc + n^2c)t$	ACC	31.30	ACC	27.82	ACC	61.11	ACC	89.81	POC	36.00
	NMI	56.56	NMI	13.42	NMI	3.48	NMI	90.76	POTC	0
	TIME	201.69	TIME	11.34	TIME	7.24	TIME	29.32	TIME	4.07
CPUFSnn [18] $O(d_1nc^2 + d_2nc^2 + d_1d_2nc + (n_1c)^2 + (n_2c)^2 + n^2c)t$	ACC	30.33	ACC	26.73	ACC	60.36	ACC	①92.46	POC	34.10
	NMI	55.05	NMI	11.21	NMI	2.86	NMI	②91.66	POTC	1.60
	TIME	106.50	TIME	11.81	TIME	8.92	TIME	20.25	TIME	4.01
STPCA-DP-1SD (ours) $O((d_1d_2)^2n + (d_1d_2)^3t)$	ACC	-	ACC	-	ACC	-	ACC	②91.69	POC	②94.67
	NMI	-	NMI	-	NMI	-	NMI	①92.66	POTC	②80.00
	TIME	-	TIME	-	TIME	-	TIME	0.62	TIME	0.01
STPCA-DP-2SD (ours) $O((d_1^2d_2n + d_1^3t_1 + d_1^2d_2n + d_2^3t_2)t)$	ACC	32.08	ACC	25.54	ACC	②63.46	ACC	90.85	POC	①100
	NMI	57.95	NMI	9.43	NMI	②4.27	NMI	89.67	POTC	①100
	TIME	0.27	TIME	0.19	TIME	0.05	TIME	4.64	TIME	0.10
STPCA-DP-MD (ours) $O((d_1d_2)^2n + (d_1d_2)^3t)$	ACC	①43.60	ACC	①34.84	ACC	61.79	ACC	90.29	POTC	73.33
	NMI	①67.79	NMI	①24.16	NMI	3.52	NMI	89.72	POTC	52.00
	TIME	5.25	TIME	219.72	TIME	1.51	TIME	376.43	TIME	2.46
STPCA-MP-Dir1 (ours) $O\left(\sum_{i=1}^{d_2} (d_1^2n + d_1^3t_i)\right)$	ACC	②42.84	ACC	②34.74	ACC	①63.87	ACC	89.13	POC	80.00
	NMI	②66.80	NMI	②23.42	NMI	①4.97	NMI	89.89	POTC	80.00
	TIME	0.03	TIME	0.06	TIME	0.02	TIME	1.75	TIME	0.05
STPCA-MP-Dir2 (ours) $O\left(\sum_{i=1}^{d_1} (d_2^2n + d_2^3t_i)\right)$	ACC	36.90	ACC	29.66	ACC	62.50	ACC	88.50	POC	80.00
	NMI	61.39	NMI	13.68	NMI	3.83	NMI	90.07	POTC	80.00
	TIME	0.03	TIME	0.05	TIME	0.02	TIME	0.11	TIME	0.04

STPCA-MP-Dir1 on PIE as an example in Fig. 6. **Both of the proposed methods converge fast.**

D. Comprehensive analysis

In this section, we connect all the experimental results on synthetic and real-world datasets and comprehensively analyze the proposed methods' application scope.

1) *Overall Conclusion:* Generally, the two STPCA-DP-SDs are more capable of tackling slice-wise tensors, while STPCA-DP-MD is more capable of dealing with tube-wise tensors. Given reasonable direction, STPCA-MP can achieve approximate performance as STPCA-DP-MD on tube-wise tensors at a significantly lower computation price. Both STPCA-DP and STPCA-MP are efficient.

2) *Detailed Analysis:* The performance of the STPCA-DP-SDs improves as the element correlations become higher,

while the situation is contrary for STPCA-DP-MD. Given different directions, STPCA-MP is sensitive to features distributed in different directions, depending on the data.

In the case of slice-wise tensors, the elements along the dimensions of 1-mode have strong correlations because of the hidden variable relations. In Orbit and UCIDSA, the elements are temporal sample values, whose structures are more constrained than UCIHAR. Therefore, the two STPCA-DP-SDs are more stable in selecting discriminative features than STPCA-DP-MD and the STPCA-MPs on Orbit and UCIDSA but don't have an obvious advantage on UCIHAR, as shown in Table IV and Table VII.

In the case of tube-wise tensors, the element correlations are reflected in the spatial distribution of features. Case 1 in Array Signal is a special situation where all features are spatially correlated. As Table V shows, the performance of the STPCA-

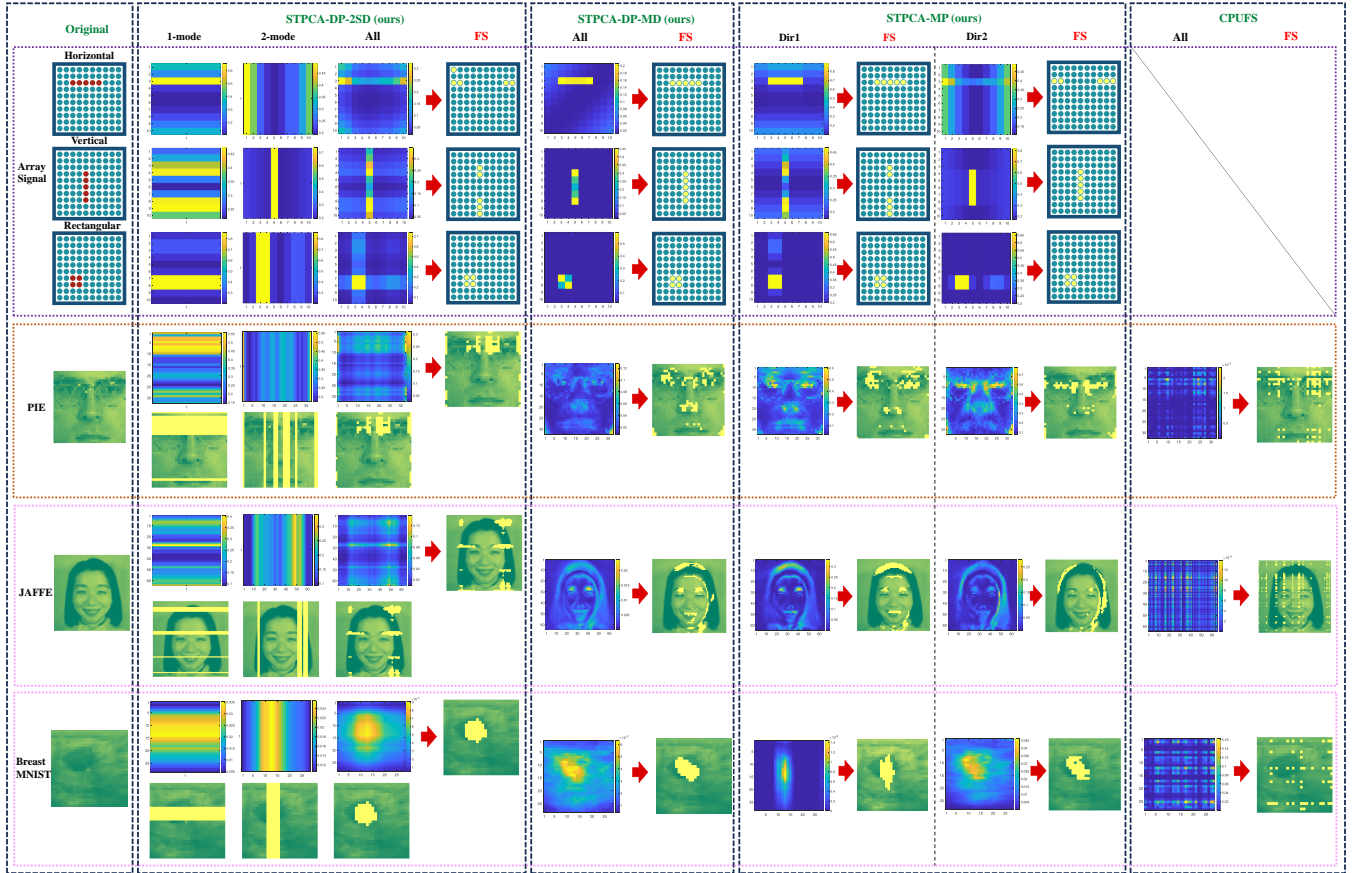


Fig. 5. Visualization on Array Signal, PIE, JAFFE, and BreastMNIST. We show the score maps and highlight the positions of the top-ranked features in the samples. We set the number of selected features to 100 on PIE, 300 on JAFFE, and 50 on BreastMNIST. Since CPUFS is not designed for complex-number data, its result on Array Signal is absent.

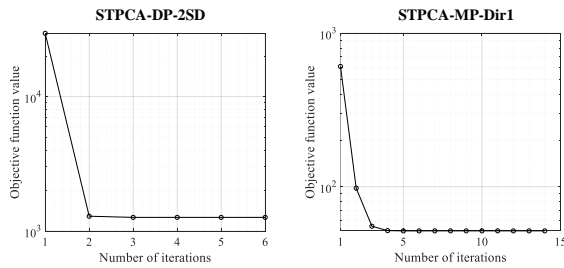


Fig. 6. Converge curves of STPCA-DP-2SD and STPCA-MP-Dir1 on PIE. All regularization parameters are set to 1. For STPCA-MP-Dir1, we retrieve the result on one of the data slices.

DP-SDs in Case 1 is close to that of the STPCA-MPs, both of which are better than the performance of STPCA-DP-MD. The multiple-direction unfolding causes the greatest structure information loss in this case. However, with measurement errors, the elements in Case 2 no longer strictly obey the structure constraints. As Table VI shows, there is a downward trend of POC for STPCA-DP-MD and an upward trend for STPCA-DP-2SD from 'Random' to 'Rectangular'. Besides, the POTC of STPCA-DP-2SD in the rectangular situation is significantly higher than that in the other situations. It can be observed that STPCA-DP-SDs tend to locate the features more

accurately as the discriminative features form a regular spatial distribution shape, while it is contrary for STPCA-DP-MD. Similar phenomena also emerge in real-world data. As Fig. 5 shows, STPCA-DP-2SD highly scores the rows (or columns) containing discriminative features in all datasets. However, only the discriminative features in BreastMNIST and the rectangular case of Array Signal are selected in the final score maps because they stick together to form an isotropic region. STPCA-DP-MD selects more discriminative features on PIE and JAFFE but has no obvious advantage on BreastMNIST. We can also see that the gap in the best ACC and NMI between these four methods is much smaller on BreastMNIST than that on PIE and JAFFE (See Table VII). As for STPCA-MP, the choice of direction leads to attention to features with different distribution directions. It can be seen that the highest POTC exists in different situations for STPCA-MP-Dir1 and STPCA-MP-Dir2 in Table VI. Besides, the ACC and NMI of these two methods differ significantly on PIE and JAFFE in Table VII. It should be noted that the focused direction is also determined by the data itself and doesn't have a fixed pattern. In general, STPCA-MP can achieve approximate or even better performance than STPCA-DP-MD at a much smaller computation price given a reasonable direction (See Table VII).

VI. CONCLUSION

In this paper, we propose two Sparse Tensor PCA methods: STPCA-DP and STPCA-MP, based on Tucker's and T-SVDs' frameworks respectively. By directly utilizing the sparse principal components of data to perform UFS, they can make greater use of tensor structure information and select more interpretable and discriminative features. The experimental results on synthetic and real-world data show that our methods outperform some state-of-the-art methods and can handle different data organization scenarios at a smaller average computation cost.

REFERENCES

- [1] H. Liu, *Feature Selection for Knowledge Discovery and Data Mining (The Springer International Series in Engineering and Computer Science)*. Springer, 1998.
- [2] R. O. Duda, P. E. Hart, and D. G. Stork, *Pattern Classification*. Wiley-Interscience, 2012.
- [3] Z. Li, F. Nie, D. Wu, Z. Wang, and X. Li, "Sparse trace ratio lda for supervised feature selection," *IEEE transactions on cybernetics*, pp. 1–14, 2023.
- [4] D. S. Z. L. C. Liu, "Binary label learning for semi-supervised feature selection," *IEEE Transactions on Knowledge and Data Engineering*, pp. 2299–2312, 2023.
- [5] X. Li, H. Zhang, R. Zhang, and F. Nie, "Discriminative and uncorrelated feature selection with constrained spectral analysis in unsupervised learning," *IEEE Transactions on Image Processing*, vol. 29, pp. 2139–2149, 2020.
- [6] R. Bellman, "Dynamic programming," *Science*, vol. 153, no. 3731, pp. 34–37, 1996.
- [7] R. Costantini, L. Sbaiz, and S. Susstrunk, "Higher Order SVD Analysis for Dynamic Texture Synthesis," *IEEE Transactions on Image Processing*, vol. 17, no. 1, pp. 42–52, Jan. 2008.
- [8] J. Shi, F. Wen, and T. Liu, "Nested MIMO Radar: Coarrays, Tensor Modeling, and Angle Estimation," *IEEE Transactions on Aerospace and Electronic Systems*, vol. 57, no. 1, pp. 573–585, Feb. 2021.
- [9] D. Wang, Y. Zheng, and G. Li, "High-dimensional low-rank tensor autoregressive time series modeling," *Journal of Econometrics*, vol. 238, no. 1, p. 105544, Jan. 2024, publisher: North-Holland.
- [10] A. Weiss, "Blind Direction-of-Arrival Estimation in Acoustic Vector-Sensor Arrays via Tensor Decomposition and Kullback-Leibler Divergence Covariance Fitting," *IEEE Transactions on Signal Processing*, vol. 69, pp. 531–545, 2021.
- [11] X. Gong, W. Chen, L. Sun, J. Chen, and B. Ai, "An ESPRIT-Based Supervised Channel Estimation Method Using Tensor Train Decomposition for mmWave 3-D MIMO-OFDM Systems," *IEEE Transactions on Signal Processing*, vol. 71, pp. 555–570, 2023.
- [12] L. D. Lathauwer, B. D. Moor, and J. Vandewalle, "A Multilinear Singular Value Decomposition," *SIAM Journal on Matrix Analysis and Applications*, Jul. 2006, publisher: Society for Industrial and Applied Mathematics.
- [13] T. Sim, S. Baker, and M. Bsat, "The cmu pose, illumination, and expression database," *IEEE Transactions on Pattern Analysis and Machine Intelligence*, vol. 25, no. 12, pp. 1615–1618, 2004.
- [14] G. Zhou, Q. Zhao, Y. Zhang, T. Adali, S. Xie, and A. Cichocki, "Linked Component Analysis From Matrices to High-Order Tensors: Applications to Biomedical Data," *Proceedings of the IEEE*, vol. 104, no. 2, pp. 310–331, Feb. 2016.
- [15] J. Zhang, M. Liu, P. Xiong, H. Du, J. Yang, J. Xu, Z. Hou, and X. Liu, "Automated Localization of Myocardial Infarction From Vectorcardiographic via Tensor Decomposition," *IEEE Transactions on Biomedical Engineering*, vol. 70, no. 3, pp. 812–823, Mar. 2023.
- [16] F. Cong, Q.-H. Lin, L.-D. Kuang, X.-F. Gong, P. Astikainen, and T. Ristaniemi, "Tensor decomposition of EEG signals: A brief review," *Journal of Neuroscience Methods*, vol. 248, pp. 59–69, Jun. 2015.
- [17] J. Levin, "Three-mode factor analysis," *Psychological Bulletin*, vol. 64, no. 6, pp. 442–452, 1965.
- [18] B. Chen, J. Guan, and Z. Li, "Unsupervised Feature Selection via Graph Regularized Nonnegative CP Decomposition," *IEEE Transactions on Pattern Analysis and Machine Intelligence*, vol. 45, no. 2, pp. 2582–2594, Feb. 2023.
- [19] C. Liang, L. Wang, L. Liu, H. Zhang, and F. Guo, "Multi-view unsupervised feature selection with tensor robust principal component analysis and consensus graph learning," *Pattern Recognition*, vol. 141, p. 109632, Sep. 2023.
- [20] H. Kuang, L. Chen, L. L. H. Chan, R. C. C. Cheung, and H. Yan, "Feature Selection Based on Tensor Decomposition and Object Proposal for Night-Time Multiclass Vehicle Detection," *IEEE Transactions on Systems, Man, and Cybernetics: Systems*, vol. 49, no. 1, pp. 71–80, Jan. 2019.
- [21] L. R. Tucker, "Some mathematical notes on three-mode factor analysis," *Psychometrika*, vol. 31, no. 3, pp. 279–311, Sep. 1966.
- [22] J. D. Carroll and J.-J. Chang, "Analysis of individual differences in multidimensional scaling via an n-way generalization of "Eckart-Young" decomposition," *Psychometrika*, vol. 35, no. 3, pp. 283–319, Sep. 1970.
- [23] R. A. Harshman, "FOUNDATIONS OF THE PARAFAC PROCEDURE: MODELS AND CONDITIONS FOR AN "EXPLANATORY" MULTI-MODAL FACTOR ANALYSIS," *UCLA Working Papers in Phonetics*, vol. 16, pp. 1–84, 1970.
- [24] M. E. Kilmer and C. D. Martin, "Factorization strategies for third-order tensors," *Linear Algebra and its Applications*, vol. 435, no. 3, pp. 641–658, Aug. 2011.
- [25] M. A. O. Vasilescu and D. Terzopoulos, "Multilinear Analysis of Image Ensembles: TensorFaces," in *7th European Conference on Computer Vision (ECCV 2002)*, 2002.
- [26] Haiping Lu, K. Plataniotis, and A. Venetsanopoulos, "MPCA: Multilinear Principal Component Analysis of Tensor Objects," *IEEE Transactions on Neural Networks*, vol. 19, no. 1, pp. 18–39, Jan. 2008.
- [27] Z. Xia, Y. Chen, and C. Xu, "Multiview PCA: A Methodology of Feature Extraction and Dimension Reduction for High-Order Data," *IEEE Transactions on Cybernetics*, vol. 52, no. 10, pp. 11068–11080, Oct. 2022.
- [28] N. Hao, M. E. Kilmer, K. Braman, and R. C. Hoover, "Facial Recognition Using Tensor-Tensor Decompositions," *SIAM Journal on Imaging Sciences*, vol. 6, no. 1, pp. 437–463, Jan. 2013.
- [29] C. Ozdemir, R. C. Hoover, and K. Caudle, "2DTPCA: A New Framework for Multilinear Principal Component Analysis," in *2021 IEEE International Conference on Image Processing (ICIP)*, Sep. 2021, pp. 344–348, iSSN: 2381-8549.
- [30] R. C. Hoover, K. S. Braman, and Ning Hao, "Pose estimation from a single image using tensor decomposition and an algebra of circulants," in *2011 IEEE/RSJ International Conference on Intelligent Robots and Systems*. San Francisco, CA: IEEE, Sep. 2011, pp. 2928–2934.
- [31] E. Kernfeld, M. Kilmer, and S. Aeron, "Tensor-tensor products with invertible linear transforms," *Linear Algebra and its Applications*, vol. 485, pp. 545–570, Nov. 2015.
- [32] H. Zou, T. Hastie, and R. Tibshirani, "Sparse principal component analysis," *J. Comput. Graph. Statist.*, vol. 15, no. 2, pp. 265–186, 2006.
- [33] Z. Lai, Y. Xu, Q. Chen, J. Yang, and D. Zhang, "Multilinear Sparse Principal Component Analysis," *IEEE Transactions on Neural Networks and Learning Systems*, vol. 25, no. 10, pp. 1942–1950, Oct. 2014.
- [34] Y.-h. Taguchi and T. Turki, "Novel feature selection method via kernel tensor decomposition for improved multi-omics data analysis," *BMC Medical Genomics*, vol. 15, no. 1, p. 37, Dec. 2022.
- [35] Y. Su, X. Bai, W. Li, P. Jing, J. Zhang, and J. Liu, "Graph regularized low-rank tensor representation for feature selection," *Journal of Visual Communication and Image Representation*, vol. 56, pp. 234–244, Oct. 2018.
- [36] X. Chang, F. Nie, Y. Yang, C. Zhang, and H. Huang, "Convex sparse pca for unsupervised feature learning," *Acm Transactions on Knowledge Discovery from Data*, vol. 11, no. 1, p. 3, 2016.
- [37] S. Yi, Z. He, X. Y. Jing, Y. Li, and F. Nie, "Adaptive weighted sparse principal component analysis for robust unsupervised feature selection," *IEEE Transactions on Neural Networks and Learning Systems*, vol. PP, no. 99, pp. 1–11, 2019.
- [38] Z. Li, F. Nie, J. Bian, D. Wu, and X. Li, "Sparse pca via l2,p-norm regularization for unsupervised feature selection," *IEEE Transactions on Pattern Analysis and Machine Intelligence*, pp. 1–1, 2021.
- [39] J. Zheng, X. Zhang, Y. Liu, W. Jiang, K. Huo, and L. Liu, "Fast sparse pca via positive semidefinite projection for unsupervised feature selection," *arXiv*, 2023.
- [40] F. Nie, W. Zhu, and X. Li, "Structured graph optimization for unsupervised feature selection," *IEEE Transactions on Knowledge and Data Engineering*, vol. PP, no. 99, pp. 1–1, 2019.
- [41] M. By L. Lovasz, *Matching theory*. North-holland, 1986.
- [42] H. W. Kuhn, "The hungarian method for the assignment problem," *Naval Research Logistics*, pp. 83–97, 1955.

- [43] M. Lyons, J. Budynek, and S. Akamatsu, "Automatic classification of single facial images," *IEEE Transactions on Pattern Analysis and Machine Intelligence*, vol. 21, no. 12, pp. 1357–1362, Dec. 1999.
- [44] J. Yang, R. Shi, and B. Ni, "MedMNIST Classification Decathlon: A Lightweight AutoML Benchmark for Medical Image Analysis," in *2021 IEEE 18th International Symposium on Biomedical Imaging (ISBI)*. Nice, France: IEEE, Apr. 2021, pp. 191–195.
- [45] D. A. G. Oneto, "A public domain dataset for human activity recognition using smartphones," in *ESANN 2013 - European Symposium on Artificial Neural Networks, Computational Intelligence and Machine Learning*, 2013.
- [46] B. Barshan and K. Altun, "Daily and Sports Activities," UCI Machine Learning Repository, 2013, DOI: <https://doi.org/10.24432/C5C59F>.
- [47] I. T. Jolliffe, "Principal component analysis," *Journal of Marketing Research*, p. 513, 2002.

Junjing Zheng received the B.E degree from the Central South University of China(CSU), Changsha, in 2021. He is currently pursuing the Ph.D degree in information and communication engineering with the National University of Defense Technology(NUDT), Changsha. His research interests include machine learning, pattern analysis, and target recognition.

Xinyu Zhang received the B.S. and Ph.D. degrees from the Beijing Institute of Technology, Beijing, China, in 2011 and 2017, respectively. From 2015 to 2017, he visited the Ohio State University as a Visiting Scholar. Since 2017, he has been holding a postdoctoral position with the National University of Defense Technology. He is currently a Lecturer with the National University of Defense Technology. His research interests include machine learning, array signal processing, auto target detection, and waveform optimization.

Weidong Jiang received the B.S. degree in communication engineering and the Ph.D. degree in electronic science and technology from the National University of Defense Technology (NUDT), China, in 1991 and 2001, respectively. He is currently a Professor with NUDT. His current research interests include multiple-input multiple-output radar signal processing and radar system technology.